WILEY-VCH

DOI: 10.1002/adfm.201802266
Article type: Full paper

On the Limits of Scalpel AFM for the 3D Electrical Characterization of Nanomaterials

*Shaochuan Chen, Lanlan Jiang, Mark Buckwell, Xu Jing, Yanfeng Ji, Enric Grustan-Gutierrez, Fei Hui, Yuanyuan Shi, Mathias Rommel, Albena Paskaleva, Guenther Benstetter, Wing H. Ng, Adnan Mehonic, Anthony J. Kenyon and Mario Lanza**

S. Chen, L. Jiang, X. Jing, Y. Ji, Dr. F. Hui, Dr. Y. Shi, Prof. M. Lanza
Institute of Functional Nano and Soft Materials, Collaborative Innovation Center of Suzhou Nanoscience & Technology, Soochow University, 199 Ren-Ai Road, Suzhou, 215123, China
E-mail: mlanza@suda.edu.cn
S. Chen
Department of Electronic, Electrical and Automatic Engineering, Rovira i Virgili University, Avinguda Països Catalans 26, Tarragona, 43007, Spain
Dr. M. Buckwell, Dr. W. H. Ng, Prof. A. Mehonic, Prof. A. J. Kenyon
Department of Electronic and Electrical Engineering, University College London, Torrington Place, London WC1E 7JE, UK
Y. Ji, Prof. G. Benstetter
Deggendorf Institute of Technology, Edlmairstraße 6, Deggendorf, 94469, Germany
Dr. E. Grustan-Gutierrez
School of Engineering and Materials Science, Queen Mary University of London, Mile End Road, London E1 4NS, UK
Dr. M. Rommell
Fraunhofer Institute for Integrated Systems and Device Technology (IISB), Schottkystrasse 10, 91058 Erlangen, Germany
Prof. A. Paskaleva
Institute of Solid State Physics, Bulgarian Academy of Sciences, 72 Tzarigradsko Chaussee, 1784 Sofia, Bulgaria

Keywords: conductive atomic force microscopy (CAFM), electrical characterization, etching, reliability, scalpel atomic force microscopy (AFM)

Abstract

Conductive atomic force microscopy (CAFM) has been widely used for electrical characterization of thin dielectrics by applying a gentle contact force that ensures a good electrical contact without inducing additional high-pressure related phenomena (e.g., flexoelectricity, local heat,

scratching). Recently, the CAFM has been used to obtain 3D electrical images of thin dielectrics by etching their surface. However, the effect of the high contact forces/pressures applied during the etching on the electrical properties of the materials has never been considered. By collecting cross-sectional transmission electron microscopy images at the etched regions, it is shown here that the etching process can modify the morphology of Al_2O_3 thin films (producing phase change, generation of defects, and metal penetration). It is also observed that this technique severely modifies the electrical properties of pSi and TiO_2 wafers during the etching, and several behaviors ignored in previous studies, including i) observation of high currents in the absence of bias, ii) instabilities of etching rate, and iii) degradation of CAFM tips, are reported. Overall, this work should contribute to understand better the limitations of this technique and disseminate it among those applications in which it can be really useful.

1. Introduction

Conductive atomic force microscopy (CAFM) was invented in 1993,[1] and nowadays it has become one of the most powerful techniques to study the electrical properties of a wide range of materials and particles with nanometric lateral resolution.[2] The CAFM uses an ultrasharp tip located at the end of a cantilever to scan the surface of a sample. The radius of the tip apex (R_{TIP}) usually ranges between 2 and 200 nm, and its contact area to the sample (A_C) ranges between 1 and 100 nm^2.[2] During the scan, the topography of the sample is recorded by measuring the deflection of the cantilever (using in most cases an optical system,[2] although some instruments use a piezoresistive system[3]). The electrical measurement is normally performed by applying a potential difference between the tip and the sample, and the current flowing between them is recorded using a current-to-voltage preamplifier. Some flexoelectric,[4] piezoelectric,[5] and photoelectric[6] samples may not require the application of bias to produce currents. Therefore, the CAFM tip must be conductive, and

its conductivity and sharpness have to be maintained throughout experiments[7]—this is very challenging due to the high lateral frictions and current densities: note that the minimum current density that a CAFM can detect is 1 A cm^{-2}, as the noise level is normally ≈1 pA and the contact area is typically ≈100 nm2.[8] Within this tip/sample system, the currents registered depend on several parameters. Those that have the biggest influence are: RTIP, the contact force applied (F_C), the conductive material of the tip (typically Pt, Pt/Ir, Ti, Co, Cr, or B-doped diamond), and the relative humidity (RH) of the environment.[2,9,10]

In its origin the CAFM was mainly used to study the currents flowing across thin insulators (i.e., the CAFM tip plays the role of a nanosized electrode[1,11,12]), and still today this is one of its main applications—if the CAFM tip is placed on metallic or semiconducting surfaces the technique loses its high lateral resolution, because the lateral resistance is very small and electrons far from the CAFM tip can also be collected.[2,13] Using the CAFM several electrical phenomena of thin insulators have been analyzed, including tunneling current,[14] trap-assisted tunneling,[15] charge trapping and detrapping,[16] stress-induced leakage current,[17] soft and hard dielectric breakdown (BD),[18] and resistive switching (RS).[19] These analyses have been always performed using a gentle contact force that ensures good electrical contact without damaging the surface of the sample and/or the CAFM tip apex.[20]

In 2013, a group from the Interuniversity Microelectronics Centre (IMEC) used a CAFM tip to scratch the surface of thin insulating materials (by applying a high F_C) and simultaneously collect the current signals driven.[21] Thus, 3D current images have been constructed from multiple current maps collected at different heights (also named slices), by speculating the current values in between those planes using rendering software (e.g., 3D Slicer, Avizo).[21,22] The working principle of this technique (often referred as CAFM-based 3D electrical tomography and/or scalpel AFM) is displayed in Figure 1. In particular, scalpel AFM has been mostly used to characterize the size and currents driven by conductive nanofilaments (CNFs) across thin insulators in RS devices under an electrical

field.[21–33] It should be noted that the diameter (Ø) of these CNFs in realistic RS devices is typically ≈10 nm,[34] and that one of the most important problems is their stability, i.e., they can self-disrupt over the time[35] or when exposed to high temperatures.[36] The RS cells studied by the IMEC group using scalpel AFM have been Cu/Al_2O_3/TiN,[21,23,24] Au/Cu/Ti/Al_2O_3/TiN,[25] Al_2O_3/Cu,[26] Ta/TaO_2/Pt,[27] Ru/Hf/HfO_2/TiN,[28,29] and TiN/HfO_2/Hf/TiN,[30] and the experiments have been mainly carried out in air atmosphere, and sporadically in a vacuum of 10^{-5} mbar. It should be noted that, in all cases: i) the oxides etched were very thin (<10 nm) and amorphous, ii) the diameter of the CNFs detected was always <30 nm, and iii) the experiments were carried out using solid B-doped diamond CAFM tips in order to avoid premature tip wearing–so far this type of CAFM tips have been fabricated and commercialized only by IMEC, and their price is up to four times higher than that of standard B-doped diamond coated Si tips from other manufacturers, such as Nanoworld.[37] After that, several groups tried to reproduce these experiments in similar samples using similar solid B-doped diamond CAFM tips; however, the number of reports from other groups using scalpel AFM is still very limited. In 2015, Buckwell et al.[22] used scalpel AFM to analyze CNFs in W/SiO_X/TiN samples; however, the diameter of the CNFs observed was much wider (Ø > 500 nm), which may not correspond to that of real RS devices under normal operation. And in 2016, Luria et al.[38] used scalpel AFM to characterize polycrystalline 2.2 μm thick CdTe films for photovoltaic cells, and the granular structure of the CdTe film was successfully displayed, showing conductive grain boundaries wider than 100 nm. However, in these two works[22,38] the features studied had diameters much larger than the CNFs displayed by the IMEC group, and it is a fact that in five years no other group has reported the characterization of the 3D shape and 3D currents of nanosized CNFs (Ø <30 nm) across amorphous thin (<10 nm) oxides using scalpel AFM. A summary of all works on scalpel AFM published to date is presented in Table 1. Therefore, here we ask ourselves which are the real limits and the reproducibility of scalpel AFM technique for the 3D characterization of CNFs and other nanoscale features across ultrathin oxides for RS devices. It is also worth noting that scalpel AFM

has been also recently used to etch the surface of Si, Ge, and SiGe semiconducting wafers for microelectronics industry (in air atmosphere).[39]

While there is no question about the ability of the CAFM tip to scratch any material if sufficient F_C is applied (local etching experiments with sharp AFM tips have been done since the 1980s),[40,41] the high pressures applied may induce severe changes on the properties of the materials being etched (e.g., local-heat-induced phase change[42,43] and even material melting[44]), which could easily modify the shape and currents driven by different features below the tip apex (e.g., <30 nm wide CNFs). Moreover, the current signals collected during the etching process may compile additional contributions due to the high pressure applied during the scan (e.g., flexoelectricity,[4] thermoelectric currents[44]), which may result in overestimations of the currents registered. And furthermore, the scratching of hard materials (e.g., Al_2O_3, TiO_2) produces premature wearing of the CAFM tips, even when these are made of solid B-doped diamond.[39] In order to clarify these issues, here we conduct a thorough investigation on the effect of scalpel AFM technique when analyzing CFs of different widths, and for the first time we collect cross-sectional transmission electron microscopy (TEM) images at the etched regions. Our observations indicate that, while this technique is very useful for the characterization of wide (Ø > 300 nm) CNFs across amorphous oxides, scalpel AFM shows to have a very low reproducibility when studying narrow (Ø < 30 nm) CNFs. The reason behind this observation is that scalpel AFM introduces non-negligible changes in the morphology (e.g., phase change, defective bonding) of the materials being etched (Al_2O_3, TiO_2, and pSi). This can partially alter the properties of wide (Ø > 300 nm) CNFs, and completely disrupt small (Ø < 30 nm) CNFs. These results should contribute to clarify the real usefulness of scalpel AFM technique and promote its widespread in those applications in which it can be really useful.

2 Experimental Section

2.1. Materials

In total four different samples containing materials commonly used in RS devices (Al_2O_3, TiO_2, and Si) were analyzed using scalpel AFM: i) The first one consisted of 5 nm Al_2O_3 films deposited by atomic layer deposition (ALD) on an n^{++}Si wafer coated with 20 nm Au and 5 nm Ti, leading to an Al_2O_3/Au/Ti/SiO_X/n^{++}Si wafer (the SiO_X layer is the native oxide of the n^{++}Si wafer, which thickness is < 1 nm). The Al_2O_3 was deposited using a Cambridge Nanotech ALD system, using trimethylaluminum (TMA) as Al source and H2O as the O source. The growth temperature was 250 °C, and the deposition rate was 0.94 Å per cycle. One ALD pulse consisted of exposure to TMA for 0.015 s and wait for 5 s. The 20 nm Au and the 5 nm Ti films were deposited by electron beam evaporation (Kurt J. Lesker Company, PVD75). ii) The second one was identical to the first one, but with an Al_2O_3 thickness of 50 nm. iii) The third one consisted of a bare pSi wafe; we etched the native oxide right before the experiments by immersion in hydrofluoric acid (HF) for 10 s. This sample is especially interesting to see if the technique is applicable to the most widespread semiconducting material in the industry (also often used in RS devices too).[45] iv) And the fourth one consisted of 2 nm TiO_2 films grown by ALD on an nSi wafer. Tetrakis(dimethylamido)titanium ($Ti(NMe_2)_4$) was used as the Ti source, and H_2O as the O source. The deposition temperature was 180 °C, and the growth rate was 0.67 Å per cycle. One ALD pulse consisted of exposure to $Ti(NMe_2)_4$ for 0.1 s and wait for 8 s.

2.2. Equipment

Different CAFMs were used in this study, including: i) Dimension Icon AFM from Bruker working in an air environment; the RH of the environment ranged around 30–40%. ii) Dimension 3100 AFM from Veeco working in air environment (RH ≈ 60%). iii) MultiMode V AFM from Veeco

working in air (RH ≈ 60%) and N_2 atmospheres (RH ≈ 0.5%). The N_2 chamber used in the MultiMode V AFM is described in ref. [46], and using this setup RH was always <0.5%, which ensured the absence of a water film on the surface of the tip and the sample. At such humidity the water layer on the surface of the tip and the sample was mostly removed, similar to what happens when working at vacuum levels of 10−5 mbar. It is emphasized here that most scalpel AFM measurements in the literature were carried out in air atmosphere (see Table 1); therefore, if one wants to analyze the reliability of this technique, the experiments need to be carried out in the same conditions. Moreover 95% of the works published with CAFM were carried out in air atmosphere; therefore, if one aims to widespread the use of scalpel AFM, its reliability concerns need to be also analyzed in air atmosphere. However, it is highlighted that the most critical analysis of this investigation (the TEM images) was carried out using samples etched under dry nitrogen atmosphere (RH < 0.5%), meaning that they would reflect the real effect of the technique without moisture artifacts being involved. In all the experiments, the bias (if any) was always applied to the sample holder, while keeping the CAFM tip grounded. When measuring in air, the voltage (V) applied to the sample substrate was always negative in order to avoid local anodic oxidation of the surface of the samples.[41]

The probe tips used in this experiment were B-doped solid diamond probes fabricated at IMEC (model SSRM-DIA); these tips contained three different cantilevers: short (≈225 μm), medium (≈305 μm), and long (≈465 μm), corresponding to nominal spring constants of 27, 11, and 3 N m^{-1} (respectively) that could range between 14–47, 5–19, and 1–6 N m^{-1} (respectively). According to the manufacturer, the value of R_{TIP} ranged between 5 and 20 nm depending on the CAFM tip used.

The effect of scalpel AFM etching process in the samples above described was analyzed in depth by collecting cross-sectional TEM images of fresh and etched areas. To do so, a focused ion beam (FEI company, model: HELIOS NANOLAB 450S) was used to cut thin lamellas, which were placed on copper grids for TEM inspection (JEOL company, model: JEM-2100). The chemical composition of the samples was analyzed by electron dispersive X-ray spectroscopy (EDS), which

was integrated in the TEM. The Al_2O_3 samples characterized using TEM/EDS were protected with 15 nm Au immediately after the CAFM etching, and right before the TEM inspection with another 15 nm C and 20 nm Cr (on top of the Au film) to enhance the contrast in the TEM image. The pSi samples characterized using TEM/EDS were only coated with 15 nm C and 20 nm Cr immediately before the TEM inspection.

2.3. Description of the etching process

2.3.1. Estimating F_{ETCH}

The first that needs to be done when starting the 3D characterization of a nanomaterial using scalpel AFM is to estimate which is the minimum F_C that starts to produce etching for the specific tip used. Here, this value is named F_{ETCH}, because the term threshold force (F_{TH}) was already used in ref. [39] to refer to the transition between two different etching modes (named "sliding" and "ploughing and sliding"). F_{ETCH} depends on: i) the physical parameters of the tip and sample (Young's modulus, Poisson's ratio, hardness, surface energy), ii) the real value (not nominal) of the tip parameters (R_{TIP} and k_C), iii) the environmental conditions (the lower the RH, the higher the etching speed because the frictions are higher),[47] and iv) the model of AFM used during the scan (it is observed that parameters specific of each AFM, such as feedback sensitivity, also play a role). Therefore, calculating the value of F_{ETCH} is extremely complex because these parameters are affected by a large intrinsic variability, and so far it can only be estimated empirically.

In order to estimate $F_{ETCH,}$ first the CAFM tip was placed on an arbitrary location of a sample and one scan was applied using a very low F_C = 0.4 μN, followed by a zoom-out scan devoted to analyze if the surface of the sample was etched. For such a low F_C no etching was observed in any of the three samples analyzed (Al_2O_3, TiO_2, and pSi). Then, F_C was increased in small steps until start

observing etching in the zoom-out scan (i.e. reduction of the surface topography at the pre-scanned regions). The first value of F_C that produced etching was F_{ETCH}. Increasing F_C in smaller steps would result in a more accurate estimation of F_{ETCH}, but at the same time this would require much more time because more AFM scans need to be collected—one should not forget that AFM is a slow technique; just to give an example, the time needed for collecting one AFM scan using a scan frequency of 0.5 Hz is: 4.5 min for 128 × 128 pixels, 9 min for 256 × 256 pixels, 18 min for 512 × 512 pixels, and 36 min for 1024 × 1024 pixels. In this case, small steps of 0.1 μN were used and estimating F_{ETCH} took us between 1 and 3 h (depending on the material to etch and the tip used). It should be mentioned that increasing F_C in small enough steps is essential to warranty that the etching is performed in sliding regime, which is supposed to provide higher etching controllability.[39]

At this stage one could also estimate the etching rate (i.e., the amount of material etched per scan) of that specific CAFM tip on that specific sample and using a specific F_C.[39] As F_{ETCH}, the etching rate also depends on several experimental parameters and can only be determined experimentally. Knowing the etching rate may allow the user to control the etching depth more accurately; however, doing that is not recommended when etching hard materials because this is a destructive process that damages the CAFM tip scan after scan (e.g., loss of conductivity by particles adhesion, increase of R_{TIP}). Therefore, it may be possible that when the user finishes the characterization of the etching rate, the CAFM tip already degraded and it is useless for the investigation (then another tip needs to be used and the entire process to estimate F_{ETCH} needs to be started again). Independent studies like the one in ref. [39] may give an idea about the etching rate of a specific type of CAFM tips on a specific material under a specific F_C. Therefore, in this scalpel study the etching rate was never characterized, only F_{ETCH} was characterized.

2.3.2. Collecting the slices

Once F_{ETCH} was estimated, the 3D electrical characterization of the interesting region of the sample (i.e., the one hosting the CNFs) was started following the process flow described in Figure 1b. First, one current map was collected on the top surface of the sample using: i) a low F_C that produces no etching (in our case < 0.4 μN), and ii) a gentle (but enough high) voltage in order to display currents across the features of interest. In this case, V = −0.2 V was used because what was supposed to be observed were the currents driven by CNFs across a thin dielectric film (i.e., −0.2 V was enough high to drive currents across the CNF, but at the same time was sufficiently low for not generating tunneling currents across the pristine dielectric). Previous works studying similar samples used voltages ranging from 10 to 500 mV (see Table 1). In ref. [38], the authors applied 0 V because they scanned polycrystalline CdTe sample and wanted to find out which are the locations that produce current.

This scan (1st read scan) corresponded to the first slice of the 3D image (depth = 0 nm). Then the same location was scanned again applying one/few scans using $F_C > F_{ETCH}$ and V = 0 V in order to produce etching (namely etching scans). All etching scans in this work were collected without applying any bias in order to produce the lowest degree of damage possible to the sample during the etching; however, previous reports on scalpel AFM used small voltages <100 mV,[21–31] which may be also acceptable. It is also important to highlight that the scan line density during the etching scans was always ≥ 256 lines μm^{-1}, which is a recommended value that reduces the distance between the etching lines, and should reduce the surface roughness of the etched region.[39] After that, another read scan (F_C < 0.4 μN and V = −0.2 V) was applied (second slice). In order to understand what is the depth that corresponds to that slice, the reading scans could be slightly larger than the etching scans, so that the nonetched part of the sample can be visualized and the height of the edge can be evaluated. The number of etching scans to apply between two reading scans (slices) will depend on the depth required to etch between two vertical slices. In principle, one could think that the more slices the better (higher accuracy); however, that would lead to very long etching times, which could

bring associated additional problems, such as prohibitive lateral drift and vertical misalignments of the slices.

The depth of the etched region could be controlled by applying a higher F_C and/or collecting a larger number of scans. However, it is important to understand that the degree of controllability of the etching process may be enough for some applications in which large depths need to be etched and in which materials' thickness fluctuations do not generate large conductivity variations (e.g., etching of bulk semiconductors,[39] and/or thick polycrystalline interlayers of solar cells)[38]; however, such degree of controllability of the etching process may be insufficient for some applications aimed to etch very thin materials in which minimal thickness fluctuations can increase the current exponentially (e.g., currents across ultrathin dielectrics).

2.3.3. Tip-to-tip variability

The etching experiments were repeated at several different fresh locations of the samples using different new tips, and it was observed that, for the same F_C applied, some tips were unable to etch the surface of the samples, while some others etched, leading to squared areas with remarkable different depths. As an example, for four different new short-cantilever solid B-doped diamond tips F_{ETCH} of 1.98, 2.12, 3.56, and 4.90 μN were estimated (under identical environmental conditions). The different etching ability observed when using different CAFM tips of the same type should be related to the variability of R_{TIP} from one tip to another, which can range between 5 and 20 nm according to the manufacturer, plus additional uncontrollable parameters, such as microroughness at the surface of the CAFM tips.[48] This variability produces that, for two different tips, the same F_C would produce two different F_{ETCH} and etching rates. Therefore, predicting F_{ETCH} and the etching rate of a CAFM tip on the surface of pSi before starting the experiment is extraordinarily complex.

Another important variability factor in CAFM tomography was the amount of debris generated during the etching scan. Sometimes it was observed that the amount of debris was negligible; however, sometimes important amount of debris appeared surrounding the etched region even if identical F_C and scanning parameters (i.e., scan size, scanline density, tip speed, integral gain, proportional gain, and voltage) were applied (see Figure S1, Supporting Information). Overall, it is concluded that the amount of debris generated and their accumulation on/by the etched region is uncontrollable and unpredictable.

3. Etching Al_2O_3

3.1. Analysis of CNFs with different diameters

The 5 nm Al_2O_3/Au/Ti/SiO_X/n^{++}Si sample was fixed on the CAFM sample holder using conductive silver paint. On one hand, the CNFs were generated using a MultiMode V AFM from Veeco (working in a N_2 atmosphere, RH ~0.5%) connected to an external Keithley 6430 source meter, which allowed measuring currents from pA up to mA, and also to set up different current limitations (CLs) during spectroscopic current versus voltage (I–V) curves. And on the other hand, the 3D electrical characterization was performed using the standard linear current-to-voltage preamplifier from the manufacturer (also called CAFM module), as that is needed to collect the current maps (slices). The switching between source meter and CAFM module was done through a homemade switch, so that the tip could be kept at the same location of the sample during both operations. Using this setup, CNFs with different diameters ranging between 10 nm and 300 nm have been formed across the 5 nm Al_2O_3 film by applying an I–V curve at different locations using different CLs (ranging from 1 μA to 1 mA)—previously it was demonstrated that the diameter of a CNF and across an amorphous oxide increases with the CL.[49] After CNF formation, the same area has been etched

using the process described in Section 2.3, by applying two etching scans (under F = 2.35 μN and V = 0 V) between each read scan (obtained under F = 0.39 μN and V = −0.2 V). Current maps (slices) have been obtained at different depths (separated vertically from each other by ≈1.25 nm) until reaching the bottom electrode (BE). For this experiment we used SSRM-DIA tips from IMEC (medium cantilever). More experimental details about all the etching experiments performed in this investigation are described in Table 2.

Figure 2a shows the five slices collected when etching a region in which a CNF was previously formed via I–V curve, using CL = 1 mA (see Figure S2a, Supporting Information). The location where the I–V curve was applied is indicated with a white cross in the 1st slice. Initially the diameter of the CNF is ≈310 nm (1st slice), which is slightly larger than that previously reported for similar Al_2O_3 samples,[50] probably due to the use of a larger CL (1 mA) used during the I–V curve. As the etching proceeds, the size of the CNF decreases (2nd–4th slice). During the 5th slice, the image appears full of current, indicating that the BE has been reached. The slices show a clear relationship to each other, and a continuous 3D image can be successfully recognized. The shape of the CNF is conical with the narrower part at the cathode side (BE), in agreement with previous studies reporting the migration of negative O^{2-} ions to the anode side (surface of the sample) under polarization.[51] In this case scalpel AFM successfully characterized the shape of a CNF with Ø > 300 nm.

When the initial I-V curve applied used CL = 10 μA (see supplementary Figure S2b), the diameter of the CNF observed in the 1st slice was only ≈26 nm (see Figure 2b, 1st slice). Interestingly, during the etching process the CNF completely vanished (see blue dashed circle in 2nd slice), showing the absence of current at that location. However, we are 100% sure that the filament was completely (not partially) formed across the entire Al_2O_3 because: i) the backward I–V curve shows Ohmic contact (see Figure S2b, Supporting Information); and ii) the first read scan shows very clearly the formation of a CNF. Re-oxidation of the CNF with the time with oxygen ions from the environment is improbable because the experiments are performed in N_2 atmosphere (RH ≈ 0.5%).

We further discarded such hypothesis because sequences of read scans applying low $F_C < 0.4$ μN on similar CNFs showed currents even after more than 3 h. Therefore, the disappearance (disruption) of the CNF is unequivocally related to the high F_C applied during the etching scans.

It is worth noting that the current pattern of the 2nd slice had no relationship with the 1st one, and that the current spots in the 3rd and 4th slices show random current distributions. The shape and distribution of the conductive features observed in the 4th slice (at the end of the etching process) show granular patterns similar to those observed in 10 nm thick polycrystalline Al_2O_3 films.[16] Therefore, Figure 2b suggests that the morphology of the Al_2O_3 may have changed during the etching process due to the high F_C applied, which is known to increase the local temperature; this high local temperature may produce the disruption of the narrow (Ø < 30 nm) CNF. It is worth noting that the physical characteristics of the tip/sample junction during the etching show strong similarities to the particle/sample junction in conventional physical sputtering, which is a widely studied subject.[52,53] Therefore the literature in this field can provide important insights on the dynamics of the problem at hand. In the field of physical sputtering it is widely known that accelerated nanoparticles (with similar length scale as the apex of the AFM tips,

These experiments were repeated at three different locations, and we observe that all wide (Ø >300 nm) CNFs formed using CL = 1 mA survived to the etching process, while all narrow (Ø <30 nm) CNFs formed using CL = 10 μA self-disrupted. This observation seems to be in contradiction to that reported in refs. [21,23–25,27–31]; however, in those works the CNFs were formed at the device level, and the top electrode was etched with the CAFM tip too. One possibility may be that the high local temperatures during the etching of the top electrode might have disrupted the CNF even before the CAFM tip reaches the surface of the oxide, and that the conductive spots displayed in the subsequent slices may not correspond to the shape of the CNF formed across the oxide during the electrical stress. More studies to clarify this issue are required. The minimum CNF size fully observable in 3D using scalpel AFM may vary from one lab to another depending on the

equipment used and the skills of the researchers to select the proper parameters during the etching; however, our study (Figure 2) demonstrates that, for identical conditions, the reliability of scalpel AFM technique reduces a lot when the size of the features analyzed reach tens of nanometer.

3.2. TEM analysis of etched regions

In order to analyze the effect of scalpel AFM on the Al_2O_3 film, the surface of a 50 nm Al_2O_3/Au/Ti/SiO_x/n^{++}Si has been etched using a Multimode V AFM working in N_2 atmosphere (RH < 0.5%). For this experiment we used a new B-doped solid diamond tip. First, a 1 μm × 1 μm reading scan has been applied using F_C = 0.39 μN and V = 0 V. Second, a 1 μm × 1 μm etching scan has been applied using $F_C = F_{ETCH}$ = 6.28 μN (sliding regime) and V = 0 V. And third, a 3 μm × 3 μm reading scan has been applied using F_C = 0.39 μN and V = 0 V. In this experiment we selected 50 nm thick Al_2O_3 film to allow better TEM characterization—several studies used RS media with a thickness of 50 nm or higher.[34] The etching scans in this experiment are small (1 μm × 1 μm), in order to be able to observe the entire etched region in the TEM image, and also to keep a high scanline density of 256 lines μm^{-1}. Figure 3a shows the topographic map collected during the third (zoom-out read) scan. Right after the etching, a 15 nm thick Au film was evaporated on top in order to passivate the surface from any potential contamination. This is a precaution commonly adopted in several TEM studies.[55,56] Moreover, as that sandwiches the Al_2O_3 film between two Au layers, identifying it in the TEM images is much easier. Before FIB and TEM experiments 15 nm C and 20 nm Cr were also deposited on the Au/Al_2O_3/Au/Ti/SiO_x/n^{++}Si sample to enhance the contrast (see Figure 4a–d).

The sample has been cut along the A–A' line in Figure 3a using a FIB, and the thin lamella has been placed on a metallic grid for TEM inspection. Figure 3b shows the TEM image of that lamella. Surprisingly, at the center of the cut (thin area), exactly below the edge of the scratched area, a long dark trace propagating into the substrate can be observed (highlighted with the yellow arrow).

This trace (see also Figure S3, Supporting Information) has only been observed in the samples exposed to CAFM tip etching, and it was never detected when cutting fresh (nonetched) samples (see Figure 3c). Therefore, this observation is not related to the sample preparation process by FIB, but to the CAFM etching process. Closer TEM inspection (Figure 4d) confirms the correct structure of the sample: the contrast between all layers is good, and the etched region can be clearly and entirely identified.

The Al_2O_3 film is very clean and homogeneous outside the etched areas (see Figure 4e and supplementary Figure S4), but near the edges and below the etched region the Al_2O_3 film shows the presence of several dark particles embedded (see also Figure 4f–k). The EDS characterization (see Figure S5, Supporting Information) displays no change on the materials composition, indicating that the main change into the Al_2O_3 may be related to its phase. Figure 4g–i shows the formation of a crystalline cone-like feature inside the amorphous Al_2O_3 film. This feature is strikingly similar to that observed in other transition metal oxides for phase change memories.[57] The high temperatures generated during the local etching may produce phase changes in the material: from amorphous (as-grown) to polycrystalline. This is consistent with previous studies in the field of crystallization of thin Al_2O_3 films,[58] which demonstrated that nucleation and crystal growth can take place due to the high temperatures (below the melting point). Another possibility may be that the polycrystalline structures observed in Figure 4g–i could be the result of the Al_2O_3 film melting and cooling at a slow rate.[59]

It should be highlighted that polycrystalline Al_2O_3 thin films are much more inhomogeneous than amorphous ones, [16] i.e., the current across the grain boundaries is much larger than across grains. However, according to Figure 4g–k, it seems that polycrystallization is not the only change induced in the Al_2O_3 film. For example, Figure 4j shows regions with severe defective bonding (which may promote trap-assisted-tunneling), and the dark areas in Figure 4k seem to indicate metal penetration into the Al_2O_3 film. As no metal migration was observed with EDS (see Figure S5, Supporting

Information), it might be possible that metal penetration occurred in quantities below the detection limit of the instrument.

4. Etching pSi wafers

The effect of local etching using scalpel AFM has been also analyzed in pSi wafers. Although this sample is not a RS structure *per se*, the study of Si wafers is important because it is a common microelectronics substrate, and it has also been used as a substrate for RS devices.[45] These experiments have been performed in air in order to match the conditions in Ref. [39], so that comparisons may be allowed.

4.1. Effect of high F_C on pSi without etching

First, the surface of a pSi wafer has been scanned using a long-cantilever B-doped solid diamond tip (in a Multimode V AFM from Veeco working in air atmosphere). The first reading scan (1 μm × 1 μm, F_C = 0.36 μN and V = −1 V) shows that the surface of the pSi sample was very flat (RMS = 200 pm, in agreement with previous works),[60] and the typical current picture previously reported for Si wafers was observed (see Figure 5a,c). After that, three consecutive etching scans (1 μm × 1 μm, F_C = 1.10 μN and V = 0 V) have been applied, followed by another zoom-out reading scan (2 μm × 2 μm, F_C = 0.36 μN and V = −1 V). The topographic map collected during the zoom-out reading scan (Figure 5b) shows no surface modification, meaning that the etching scans were in fact unable to etch the surface of the pSi (i.e., F_C, was not enough high). Interestingly, the current map recorded during the 5th scan (Figure 5d) showed squared insulating areas with the same size and position as the 2nd–4th scans (which used F_C = 1.10 μN). Therefore, the 2nd–4th scans clearly increased the resistivity of the pSi wafer. It is worth noting that, if the experiment is repeated by

applying F_C < 0.4 μN during the 2nd–4th scans, the current map collected during the 5th scan does not show this conductivity reduction (i.e., it is just similar to that shown in Figure 5c). Therefore, the conductivity reduction observed in Figure 5d should be related to the higher pressures applied during the 2nd–4th scans. Unfortunately, these regions cannot be detected via SEM because they did not produce any topographic change (no etching), and therefore we could not perform FIB to analyze them via cross-sectional TEM. Whilst at this point we cannot be sure about the structural changes that the pressure applied by the CAFM tip induced in the pSi wafer, it has been demonstrated that a threshold pressure of 15 GPa applied on the surface of crystalline silicon can produce its amorphization without being etched significantly. By considering that the AFM tip contact area is 100 nm^2, a force of only 1.5 μN will produce an identical pressure.[61] This value is of the same order as those reported in ref. [39] for the etching of silicon. In fact, phase transitions of Si I to Si II and Si V can happen at even lower pressure values of 9–13.2 GPa. Therefore, one possible explanation for the observation in Figure 5d is that the generation of local heat at high pressures altered the crystalline structure of the silicon wafer, amorphizing the surface of the pSi wafer and leading to a current reduction (it is known that the resistivity of amorphous silicon is higher than that of crystalline silicon).[59]

Figure 5d also reveals that the CAFM has a non-negligible lateral drift (which is normal in all CAFMs). It is worth noting that the lateral drift induced during the etching scans (higher F_C), evidenced in Figure 5d by the shift of the squared insulating (blue) area, is much larger than that observed in sequences of scans using lower F_C. Ref. [39] also shows remarkable lateral drift during the etching process, which is observable even in the SEM images (see Supporting Information of ref. [39]); this means that the lateral drift in that work is not small because the lateral resolution of SEM is much lower than that of AFM. Such phenomenon is reasonable because the piezo tube of the AFM may not maintain a fixed X–Y scan center position due to the high repulsive normal force derived

from the aggressive scratching process. Therefore, this observation indicates that the CAFM etching technique could be affected by large lateral drifts.

4.2. Etching process of pSi

In order to etch the surface of the pSi wafer, the experiments have been repeated using a solid B-doped diamond CAFM tip with short-cantilever (in a Multimode V AFM from Veeco working in air atmosphere). Figure 6a shows the 1.5 μm × 1.5 μm (reading) topographic map collected by applying F_C = 0.39 μN and V = -0.5 V at a location of the pSi wafer where previously one 500 nm × 500 nm (etching) scan by applying $F_C = F_{ETCH}$ = 2.35 μN and V = 0 V was collected. The use of $F_C = F_{ETCH}$ = 2.35 μN during the etching scan implies that the etching has been carried out in sliding regime. The depth etched in the scan is ~1.5 nm (see Figure 6b), which agrees well with previous observations for such F_C in sliding regime (in this material).[39] The roughness of the pSi wafer outside the etched region is ~0.2 nm, and the roughness of the etched region is just slightly larger (~0.25 nm) but comparable. The roughness of the etched region may be reduced by increasing the number of scan lines μm^{-1}; however, one needs to be aware that this will strongly limit the area etched, or will increase a lot the etching time.

The current signals inside and outside the etched regions of the pSi sample have been compared by analyzing the current map (Figure 6c) collected simultaneously to the zoom-out reading scan (Figure 6a). As it can be observed, the pSi inside the etched region is much more insulating than the one outside, indicating that the scalpel AFM etching process has altered the properties of the pSi. We also confirm that the differences observed in Figure 6a cannot be related to the presence/absence of native SiO_X outside/inside the etched region, as we etched it right before the experiment by immersion in HF for 10 s. More details about the effect of native oxide on the etching can be found in Figure S6 (Supporting Information). Therefore, the differences observed in Figure 6c are

unequivocally related to the CAFM tip induced etching process. This phenomenon should not be ignored when using scalpel AFM to etch Si wafers.

We also would like to highlight a puzzling observation ignored in all previous scalpel AFM reports. For this specific sample (pSi), during the etching process abundant currents have been often observed even in the absence of bias. When scanning the surface of pSi with F_C = 0.39 μN the currents collected are just electrical noise, while currents > 5 pA appear when F_C > 1 μN (Video S1, Supporting Information). The currents observed during the etching can go much higher if F_C is further increased (>1 nA for F_C > 6.28 μN), as displayed in Figure S7 (Supporting Information). This behavior has been observed using different AFMs, and also when measuring in N_2 atmosphere, meaning that it is not related to a specific setup, nor to the water meniscus at the tip/sample junction. We are also sure that they are not related to any offset voltage of the CAFM, as we have characterized it to be −2.25 mV (see Figure S8, Supporting Information), and this voltage is unable to produce any current in pSi wafers (only shows currents in pure metallic samples and ohmic contacts). The observation of high currents when scanning pSi wafers under high F_C may be related to flexoelectric, piezoelectric and/or thermoelectric currents derived from the high F_C applied during the etching.[4,5] Further studies should clarify the origin of such a current signal (which is out of the scope of this work). In any case, this behavior further confirms the generation of additional electronic phenomena during the etching, which may affect the material below and the measured current signals relating to the conductive features under investigation.

5. Etching TiO_2 thin films

According to our experiments, the etching of a material using the CAFM tip can alter not only the electrical resistance of the sample, but also other electro-physical properties. In the next experiment the surface of a 2 nm TiO_2/nSi sample has been scanned with a Dimension 3100 AFM

working in air atmosphere, using a short-cantilever B-doped solid diamond tip. A 1 μm × 1 μm scan has been applied on a random position of the sample by applying F_C = 0.51 μN and V = 0 V. The topographic map (Figure 7a) shows that the surface of the TiO_2 film is very flat (RMS < 300 pm), and the current map (Figure 7d) shows the presence of current without applying bias. It should be highlighted that this phenomenon is different to the one discussed in Section 3.2 (Figure S7, Supporting Information), as in this scan no high force has been applied. Although this observation is unusual, we know well that this current is related to the photoelectric effect in the TiO_2/nSi sample when exposed to the light bank and the laser of the CAFM.[62] This conclusion was obtained by measuring the sample in an AFM without laser (the Multimode 4000 from Nanonics) under complete dark conditions (i.e., light bank was switched off and the CAFM was covered to protect the sample from room light).[62] At the same location, another 1 μm × 1 μm scan with F_C = 1.10 μN and V = 0 V was applied in order to etch the surface of the TiO_2, followed by a zoom-out 2 μm × 2 μm (using F_C = 0.51 μN and V = 0 V) to characterize the depth and conductivity of the etched area. As it can be observed, the depth of the etched region is <1 nm (see Figure 7c), as confirmed by the cross-section analysis of scan 3 (see Figure S9, Supporting Information). The current map collected during the third scan on the etched 2 nm TiO_2/nSi sample (Figure 7f) shows that the etched area (containing 1 nm TiO_2) shows no photocurrent. This observation indicates that the CAFM tomography technique altered the properties of the TiO_2 film during the etching.

3.4. Degradation of the CAFM tips

When aiming for 3D electrical characterization via scalpel AFM the tip apex must remain sharp and conductive for the duration of the measurement in order to ensure reliable electrical data collection. If soft materials are etched (such as polymers[63]), wearing of the tip (e.g., bulk material removal and reduction of its sharpness) may not be a concern. However, etching hard materials (e.g.,

Al_2O_3, pSi) will wear the tip after a certain number of scans, even if it is made of solid diamond. To investigate the different degradation modes of CAFM tips during etching, we performed SEM on B-doped solid diamond probes that had been used to varying degrees to etch sputter-deposited and spin-on SiO_X films, as used in some resistive switching devices.[64,65] Figure 8a,b shows the top-view and side-view SEM images of a pristine probe (respectively), demonstrating its sharpness, with an apex around 20 nm. Figure 8c,d shows a probe that has been used to etch sputter-deposited SiO_X. The total distance travelled by the tip was 18 mm, i.e., 24 scans with a size of 2 µm × 2 µm and 256 lines per scan, under F_C of 3.5 and 7.1 µN, each for half the total distance. Here, the apex appears obscured by a relatively small piece of debris. This would suggest that the probe would become insulating and etch more slowly as it is less sharp. Interestingly, however, the resistance of the probe decreased by around 7 kΩ following etching and its removal rate increased by around 20% over the course of the etching. If the experiments proceed, it is not difficult to arrive to a point in which the number of debris on the tip apex is prohibitive, and the tip loses its conductivity, i.e., does not show currents anymore even if the maximum bias allowed by the CAFM (± 10 V) is applied (see Figure 8e). Here, the apex is obscured, suggesting that this probe would no longer be sharp or conductive (assuming the debris is insulating, as it should be composed of SiO_X). Similarly, Figure 8f shows a different probe that has been used to scan the surface of spin-on SiO_X. The apex is no longer point-like, so is likely not sharp. However, there is not much debris at the apex, so this probe might still be conductive. Its contact area would be significantly larger than that of a pristine probe, and therefore the current measured might increase.[2] For the degraded probes in Figure 8e,f, it is not clear whether the degradation occurred gradually or at a distinct point during measurement. Both probes were used in etching for up to tens of millimeter at estimated applied forces of up to around 10 µN. The B-doped solid diamond tips used in Figure 8e,f degrade slower than nondiamond tips. It would be beneficial if all researchers using this technique indicate the distance travelled by the CAFM tips as well as the F_C used before claiming if the tips degrade slow or fast.

In cases of probe wear, without performing SEM it is difficult to know the geometry of the apex. Thus, significant degradation might occur without the experimenter being aware of such changes. As such, the reliability of the tomography data may degrade scan after scan. In particular, the current measurements will be skewed by changes in contact resistance and geometry, thus the probe would convolute the shape of conductive features (such as CNFs). Given that B-doped solid diamond probes are expensive compared to metal and B-doped diamond coated probes, it is likely that they would be required for multiple measurements and so probe degradation would almost certainly occur to some extent.

Another puzzling observation when using scalpel AFM is the observation of sudden and random decreases and increases of the etching capability of the CAFM tips. In the next experiment, a short-cantilever B-doped solid diamond tip has been used to etch the surface of the 50 nm Al_2O_3/20 nm Au/5 nm Ti/SiO_X/n^{++}Si sample at two different locations. When we started this experiment the CAFM tip was not new, but it was previously used to do some of the experiments described in Section 3.2. This experiment has been performed using the Multimode V AFM working in N_2 atmosphere.

We etched the surface of the Al_2O_3 film by applying two (1 μm × 1 μm) scans using F_C = 2.35 μN and V = 0 V, and one additional (2.5 μm × 2.5 μm) zoom-out scan was collected using F_C = 0.39 μN and V = 0 V in order to monitor the depth of the area etched. Figure 8e (black line) shows the cross-sectional analysis of the last topographic map, and it can be concluded that the depth of the etched region ranges between 6 nm and 12 nm. It should be noted that the cross-section has been done perpendicular to the scan direction, meaning that the left/right of the X-axis correspond to the first/last scan line (see numbers on the top X-axis). Right after that, the experiment is repeated on a different fresh location of the sample with a lower F_C = 1.77 μN during the etching scans. Initially the etching rate is the same, but at around line 110 (of 256), the depth of the etched region suddenly increased. It should be highlighted that the F_C = 1.77 μN was constant during the entire scan. The only feasible explanation for such observation is that one particle attached to the tip during the first

experiment (black line in Figure 8e) detached during the etching scan, reducing AC and increasing the etching rate, leading to deeper etching during the subsequent scan lines. In fact, the concept of etching rate itself may not be reliable as currently defined (i.e., depth etched after a certain number of scans divided by the number scans[39]), as the depth etched changes from one scan to another (see Figure S10, Supporting Information).

5. Conclusions

In conclusion, Al_2O_3, pSi, and TiO_2 samples have been etched via scalpel AFM, and the etched regions have been analyzed via CAFM current maps and cross-sectional TEM images. The experiments show that scalpel AFM severely changes the electrical properties of pSi and TiO_2 wafers in an uncontrollable way due to the high contact forces/pressures required (even when $F_C = F_{ETCH}$ is applied). In the case of pSi wafers, even the use of $F_C < F_{ETCH}$ results in material modification. In the case of Al_2O_3, material modification (e.g., phase change, generation of defects, and metal penetration) also takes place, as confirmed via cross-sectional TEM analyses. This limits the lateral resolution of scalpel AFM technique when studying nanosized electrical features, such as CNFs for resistive switching applications. More specifically, we find that, while scalpel AFM works reasonably well when analyzing wide CNFs with Ø > 300 nm, when studying narrow CNFs with Ø < 30 nm the technique produces CNF disruption due to the high forces applied during the etching. Other nonidealities never reported before, such as the apparition of currents in the absence of bias, random changes in the etching rate due to particle adhesion, and degradation of the CAFM tip, are also discussed. In view of these phenomena, we provide an updated process flow for the correct use of scalpel AFM to characterize the electrical properties of nanomaterials in three dimensions.

Acknowledgement

This work has been supported by the Young 1000 Global Talent Recruitment Program of the Ministry of Education of China, the Ministry of Science and Technology of China (grant no. BRICS2018-211-2DNEURO), the National Natural Science Foundation of China (grants no. 61502326, 41550110223, 11661131002, 61874075), the Jiangsu Government (grant no. BK20150343), the Ministry of Finance of China (grant no. SX21400213) and the Young 973 National Program of the Chinese Ministry of Science and Technology (grant no. 2015CB932700). The Collaborative Innovation Center of Suzhou Nano Science & Technology, the Jiangsu Key Laboratory for Carbon-Based Functional Materials & Devices, the Priority Academic Program Development of Jiangsu Higher Education Institutions, and the 111 Project from the State Administration of Foreign Experts Affairs are also acknowledged. Additional support was from the Engineering and Physical Sciences Research Council, UK under grant number EP/K01739X/1, Leverhulme Trust under grand number RPG-2016-135, and The Worshipful Company of Scientific Instrument Makers.

References

[1] M. P. Murrell, M. E. Welland, S. J. O'Shea, T. M. H. Wong, J. R. Barnes, A. W. McKinnon, M. Heyns, S. Verhaverbeke, *Appl. Phys. Lett.* **1993**, *62*, 786.

[2] C. Pan, Y. Shi, F. Hui, E. Grustan-Gutierrez, M. Lanza, *Conductive Atomic Force Microscopy: Applications in Nanomaterials*, Wiley-VCH, Berlin, Germany **2017**.

[3] D. Lewis, S. K. AndreyIgnatov, R. Dekhter, A. and Strinkovsky, *Conductive Atomic Force Microscopy: Applications in Nanomaterials*, Wiley-VCH, Berlin, Germany **2017**.

[4] U. K. Bhaskar, N. Banerjee, A. Abdollahi, Z. Wang, D. G. Schlom, G. Rijnders, G. Catalan, *Nat. Nanotechnol.* **2016**, *11*, 263.

[5] C. Pan, J. Hu, E. Grustan-Gutierrez, M. T. Hoang, H. Duan, J. Yvonnet, A. Mitrushchenkov, G. Chambaud, M. Lanza, *J. Mater. Chem. C* **2016**, *4*, 3646.

[6] T. Han, S. Privitera, R. G. Milazzo, C. Bongiorno, S. Di Franco, F. La Via, X. Song, Y. Shi, M. Lanza, S. Lombardo, *Mater. Sci. Eng. B* **2017**, *225*, 128.

[7] O. M. Krause, *Conductive Atomic Force Microscopy: Applications in Nanomaterials*, Wiley-VCH, Berlin, Germany **2017**.

[8] M. Lanza, M. Reguant, G. Zou, P. Lv, H. Li, R. Chin, H. Liang, D. Yu, Y. Zhang, Z. Liu, H. Duan, *Adv. Mater. Interfaces* **2014**, *1*, 1300101.

[9] M. Lanza, M. Porti, M. Nafría, X. Aymerich, E. Whittaker, B. Hamilton, *Rev. Sci. Instrum.* **2010**, *81*, 106110.

[10] M. Lanza, M. Porti, M. Nafría, X. Aymerich, E. Whittaker, B. Hamilton, *Microelectron. Reliab.* **2010**, *50*, 1312.

[11] S. J. O'Shea, *J. Vac. Sci. Technol. B Microelectron. Nanometer Struct.* **1995**, *13*, 1945.

[12] T. G. Ruskell, R. K. Workman, D. Chen, D. Sarid, S. Dahl, S. Gilbert, *Appl. Phys. Lett.* **1996**, *68*, 93.

[13] S. Sonde, F. Giannazzo, C. Vecchio, R. Yakimova, E. Rimini, V. Raineri, *Appl. Phys. Lett.* **2010**, *97*, 132101.

[14] M. Lanza, M. Porti, M. Nafria, G. Benstetter, W. Frammelsberger, H. Ranzinger, E. Lodermeier, G. Jaschke, *Microelectron. Reliab*. **2007**, *47*, 1424.

[15] O. Pirrotta, L. Larcher, M. Lanza, A. Padovani, M. Porti, M. Nafría, G. Bersuker, *J. Appl. Phys.* **2013**, *114*, 134503.

[16] M. Lanza, M. Porti, M. Nafría, X. Aymerich, G. Benstetter, E. Lodermeier, H. Ranzinger, G. Jaschke, S. Teichert, L. Wilde, P. P. Michalowski, *IEEE Trans. Nanotechnol.* **2011**, *10*, 344.

[17] M. Lanza, M. Porti, M. Nafría, X. Aymerich, G. Ghidini, A. Sebastiani, *Microelectron. Reliab.* **2009**, *49*, 1188.

[18] N. Raghavan, K. L. Pey, K. Shubhakar, *Microelectron. Reliab.* **2014**, *54*, 847.

[19] M. Lanza, G. Bersuker, M. Porti, E. Miranda, M. Nafría, X. Aymerich, *Appl. Phys. Lett.* **2012**, *101*, 193502.

[20] G.-H. Lee, Y.-J. Yu, C. Lee, C. Dean, K. L. Shepard, P. Kim, J. Hone, *Appl. Phys. Lett.* **2011**, *99*, 243114.

[21] U. Celano, L. Goux, A. Belmonte, A. Schulze, K. Opsomer, C. Detavernier, O. Richard, H. Bender, M. Jurczak, W. Vandervorst, in *Tech. Dig. - Int. Electron Devices Meet.* IEEE, Washington, DC, **2013**.

[22] M. Buckwell, L. Montesi, S. Hudziak, A. Mehonic, A. J. Kenyon, *Nanoscale* **2015**, *7*, 18030.

[23] U. Celano, L. Goux, A. Belmonte, K. Opsomer, A. Franquet, A. Schulze, C. Detavernier, O. Richard, H. Bender, M. Jurczak, W. Vandervorst, *Nano Lett.* **2014**, *14*, 2401.

[24] U. Celano, L. Goux, A. Belmonte, K. Opsomer, R. Degraeve, C. Detavernier, M. Jurczak, W. Vandervorst, *J. Phys. Chem. Lett.* **2015**, *6*, 1919.

[25] U. Celano, L. Goux, K. Opsomer, M. Iapichino, A. Belmonte, A. Franquet, I. Hoflijk, C. Detavernier, M. Jurczak, W. Vandervorst, *Microelectron. Eng.* **2014**, *120*, 67.

[26] U. Celano, G. Giammaria, L. Goux, A. Belmonte, M. Jurczak, W. Vandervorst, *Nanoscale* **2016**, *8*, 13915.

[27] U. Celano, J. Op de Beeck, S. Clima, M. Luebben, P. M. Koenraad, L. Goux, I. Valov, W. Vandervorst, *ACS Appl. Mater. Interfaces* **2017**, *9*, 10820.

[28] U. Celano, A. Fantini, R. Degraeve, M. Jurczak, L. Goux, W. Vandervorst, *AIP Adv.* **2016**, *6*, 085009.

[29] U. Celano, L. Goux, R. Degraeve, A. Fantini, O. Richard, H. Bender, M. Jurczak, W. Vandervorst, *Nano Lett.* **2015**, *15*, 7970.

[30] U. Celano, Y. Yin Chen, D. J. Wouters, G. Groeseneken, M. Jurczak, W. Vandervorst, *Appl. Phys. Lett.* **2013**, *102*, 121602.

[31] U. Celano, *Metrology and Physical Mechanisms in New Generation Ionic Devices*, Springer International Publishing, Switzerland **2016**.

[32] U. Celano, W. Vandervorst, *Conductive Atomic Force Microscopy: Applications in Nanomaterials*, Wiley-VCH, Berlin, Germany **2017**.

[33] M. Lanza, U. Celano, F. Miao, *J. Electroceram* **2017**, *39*, 94.

[34] Z. Wang, S. Joshi, S. E. Savel'ev, H. Jiang, R. Midya, P. Lin, M. Hu, N. Ge, J. P. Strachan, Z. Li, Q. Wu, M. Barnell, G.-L. Li, H. L. Xin, R. S. Williams, Q. Xia, J. J. Yang, *Nat. Mater.* **2017**, *16*, 101

[35] A. Bsiesy, P. Gonon, C. Vallee, J. Pointet, C. Mannequin, *ECS Trans.* **2015**, *67*, 99.

[36] U. Russo, D. Ielmini, C. Cagli, A. L. Lacaita, *IEEE Trans. Electron Devices* **2009**, *56*, 193.

[37] F. Hui, P. Vajha, Y. Shi, Y. Ji, H. Duan, A. Padovani, L. Larcher, X. R. Li, J. J. Xu, M. Lanza, *Nanoscale* **2016**, *8*, 8466.

[38] J. Luria, Y. Kutes, A. Moore, L. Zhang, E. A. Stach, B. D. Huey, Charge transport in cdte solar cells revealed by conductive tomographic atomic force microscopy, *Nat. Energy* **2016**, *1*, 16150.

[39] U. Celano, F.-C. Hsia, D. Vanhaeren, K. Paredis, T. E. M. Nordling, J. G. Buijnsters, T. Hantschel, W. Vandervorst, *Sci. Rep.* **2018**, 8, 2994.

[40] O. C. Wells, *US patent US4785189* **1988**.

[41] R. Garcia, A. W. Knoll, E. Riedo, *Nat. Nanotechnol.* **2014**, *9*, 577.

[42] S. Shahin, P. Gangopadhyay, R. A. Norwood, *Adv. Opt. Mater.* **2016**, *4*, 1805.

[43] E. Grustan-Gutierrez, C. Wei, B. Wang, M. Lanza, *Cryst. Res. Technol.* **2017**, *52*, 1600240.

[44] F. Ma, Y. Ou, Y. Yang, Y. Liu, S. Xie, J.-F. Li, G. Cao, R. Proksch, J. Li, *J. Phys. Chem. C* **2010**, *114*, 22038.

[45] N. Xiao, M. A. Villena, B. Yuan, S. Chen, B. Wang, M. Eliáš, Y. Shi, F. Hui, X. Jing, A. Scheuermann, K. Tang, P. C. McIntyre, M. Lanza, *Adv. Funct. Mater.* **2017**, *27*, 1700384.

[46] Y. Ji, F. Hui, Y. Shi, T. Han, X. Song, C. Pan, M. Lanza, *Rev. Sci. Instrum.***2015**, *86*, 106105.

[47] H.-J. Butt, B. Cappella, M. Kappl, *Surf. Sci. Rep.* **2005**, *59*, 1.

[48] K. Arstila, T. Hantschel, C. Demeulemeester, A. Moussa, W. Vandervorst, Microfabricated diamond tip for nanoprobing, *Microelectron. Eng.* **2009**, *86*, 1222.

[49] H. J. Uppal, I. Z. Mitrovic, S. Hall, B. Hamilton, V. Markevich, A. R. Peaker, *J. Vac. Sci. Technol. B: Microelectron. Nanometer Struct.* **2009**, *27*, 443.

[50] L. Jiang, Y. Shi, F. Hui, K. Tang, Q. Wu, C. Pan, X. Jing, H. Uppal, F. Palumbo, G. Lu, T. Wu, H. Wang, M. A. Villena, X. Xie, P. C. McIntyre, M. Lanza, *ACS Appl. Mater. Interfaces* **2017**, *9*, 39758.

[51] G. Bersuker, D. C. Gilmer, D. Veksler, J. Yum, H. Park, S. Lian, L. Vandelli, A. Padovani, L. Larcher, K. McKenna, A. Shluger, V. Iglesias, M. Porti, M. Nafria, W. Taylor, P. D. Kirsch, R. Jammy, in *Tech. Dig. - Int. Electron Devices Meet.*, IEEE, San Francisco, CA **2010**.

[52] R. Borrajo-Pelaez, E. Grustan-Gutierrez, M. Gamero-Castaño, *J. Appl. Phys.* **2013**, *114*, 184304.

[53] M. Gamero-Castaño, A. Torrents, L. Valdevit, J.-G. Zheng, *Phys. Rev. Lett.* **2010**, *105*, 145701.

[54] M. Gamero-Castaño, M. Mahadevan, *Appl. Surf. Sci.* **2009**, 255, 20, 8556–8561, 2009.

[55] Y. Shi, T. Han, C. Gimbert-Suriñach, X. Song, M. Lanza, A. Llobet, *J. Mater. Chem. A* **2017**, *5*, 1996.

[56] T. Han, Y. Shi, X. Song, A. Mio, L. Valenti, F. Hui, S. Privitera, S. Lombardo, M. Lanza, *J. Mater. Chem. A* **2016**, *4*, 8053.

[57] D.-H. Kwon, K. M. Kim, J. H. Jang, J. M. Jeon, M. H. Lee, G. H. Kim, X.-S. Li, G.-S. Park, B. Lee, S. Han, M. Kim, C. S. Hwang, *Nat. Nanotechnol.* **2010**, *5*, 148.

[58] S. Jakschik, U. Schroedera, T. Hechta, M. Gutschea, H. Seidla, J. W. Bartha, *Thin Solid Films* **2003**, 425, 216.

[59] T. Nishikawa, K. Ohdaira, H. Matsumura, *Curr. Appl. Phys.* **2011**, *11*, 604.

[60] Y. Shi, Y. Ji, H. Sun, F. Hui, J. Hu, Y. Wu, J. Fang, H. Lin, J. Wang, H. Duan, M. Lanza, *Sci. Rep.* **2015**, *5*, 11232.

[61] M. Gamero-Castaño, M. Mahadevan, *J. Appl. Phys*. **2009**, 106, 5.

[62] Y. Ji, F. Hui, Y. Shi, V. Iglesias, D. Lewis, J. Niu, S. Long, M. Liu, A. Hofer, W. Frammelsberger, G. Benstetter, A. Scheuermann, P. C. McIntyre, M. Lanza, *Rev. Sci. Instrum.* **2016**, *87*, 83703.

[63] X. N. Xie, M. Deng, H. Xu, S. W. Yang, D. C. Qi, X. Y. Gao, H. J. Chung, C. H. Sow, V. B. C. Tan, A. T. S. Wee, *J. Am. Chem. Soc.* **2006**, 128, 2738.

[64] A. Mehonic, M. Buckwell, L. Montesi, M. S. Munde, D. Gao, S. Hudziak, R. J. Chater, S. Fearn, D. McPhail, M. Bosman, A. L. Shluger, A. J. Kenyon, *Adv. Mater.* **2016**, *28*, 7486.

[65] W. H. Ng, A. Mehonic, M. Buckwell, L. Montesi, A. J. Kenyon, *IEEE Trans. Nanotechnol.* **2018**, *17*, 884.

Received: ((will be filled in by the editorial staff))
Revised: ((will be filled in by the editorial staff))
Published online: ((will be filled in by the editorial staff))

Table 1: Use of CAFM 3D tomographhy in the characterization of resistive switching devices.

RS device structure	Tip	Atmosphere	Voltage	CNF diameter	Ref.
W/37 nm SiO*x*/TiN (amorphous)	Diamond coated (B-doped) Si tip k = 6 N/m	Air	50 mV to sample (tip grounded)	Hundreds nanometer	[22]
Cu/5nm Al_2O_3/TiN (amorphous)	B-doped solid diamond tip k = 10 / 30 N/m	*Not specified*	≈ -10 mV to sample (tip grounded)	14 – 22nm	[23]
Cu/5nm Al_2O_3/TiN (amorphous)	B-doped solid diamond tip k ≈ 30 N/m	*Not specified*	*Not specified*	≈ 21 nm, ≈ 29 nm	[24]
Au/Cu/Ti/3nm Al_2O_3/TiN (amorphous)	B-doped solid diamond tip *k not specified*	*Not specified*	*Not specified*	30 – 50 nm	[25]
5nm Al_2O_3/Cu (amomrphous)	B-doped solid diamond tip *k not specified*	High vacuum (≈ 10^{-5} mbar)	*Not specified*	7.8 – 17 nm	[26]
Pt/Ta/5nm TaO_2/Pt (not specified)	B-doped solid diamond tip k > 10 N/m	Air	500 mV to sample (tip grounded)	Tens nanometer	[27]
Ru/Hf/5nm HfO_2/TiN (amorphous)	B-doped solid diamond tip k ≈ 10 N/m	High vacuum (≈ 10^{-5} mbar)	*Not specified*	6.2 – 10nm	[28]
Ru/Hf/5nm HfO_2/TiN (amorphous)	B-doped solid diamond tip k ≈ 30 N/m	High vacuum (≈ 10^{-5} mbar)	≈ 100 mV positive polarity to tip	2.8 – 6.2nm	[29]
TiN/10nm HfO_2/Hf/TiN (not specified)	B-doped solid diamond tip k = 30 – 50 N/m	N_2	*Not specified*	5 – 10nm 30 – 50nm	[30]
2.7µm CdTe/120nm CdS/FTO (polycrystalline)	Diamond-coated silicon probe (k = 40N/m)	Air	0 V/0.7V tip bias	Not applicable	[38]
Si, Ge and SiGe	B-doped solid diamond tip k = 10 N/m	Air	*Not specified*	Not applicable	[39]

Table 2: Details of all the etching experiments performed in this investigation. "R" denotes reading scan, which has been carried out using a low contact force. "E" denotes a scan applied with a higher contact force that intends to etch the sample. The scanline density was always >256 lines/µm, which is a value recommended in Ref. [39] for low surface roughness. All the etchings in this work have been carried out using a force slightly larger than F_{ETCH} (sliding mode), meaning that the material modification observed in Figures 2-7 could not have been avoided by using a lower (more gentle) contact force. In Figure 5 material modification has been observed even when applying $F_C < F_{ETCH}$. In Figures 2a and 2b, the experiment consisted on 13 scans. The 5th-6th, 8th-9th and 11th-12th scans (etching) scans used the same parameters than the 2nd-3rd scans, and the 7th, 10th and 13th scans (reading) scans used the same parameters than the 4th scan.

Figures	**Sample**	**Tip**	**R = 1st scan**	**E = 2nd-3rd scan**	**R = 4th scan**	**Environment**
Figure 2a*	5 nm Al_2O_3/ Au/Ti/SiO_X /n^{++}Si	k = 27 N/m	1.6 µm × 1.6 µm F_C = 0.39 µN V = -0.2 V	1.4 µm × 1.4 µm F_C = 2.35 µN V = 0 V	1.6 µm × 1.6 µm F_C = 0.39 µN V = -0.2 V	N_2 (RH < 0.5%)
Figure 2b*	5 nm Al_2O_3/ Au/Ti/SiO_X /n^{++}Si	k = 27 N/m	0.18 µm × 0.18 µm F_C = 0.39 µN V = -0.2 V	0.2 µm × 0.2 µm F_C = 2.35 µN V = 0 V	0.3 µm × 0.3 µm F_C = 0.39 µN V = -0.2 V	N_2 (RH < 0.5%)
			R = 1st scan	**E = 2nd scan**	**R = 3rd scan**	
Figure 3a, b,4	50 nm Al_2O_3/ Au/Ti/n^{++}Si	k = 27 N/m	1 µm × 1 µm F_C = 0.39 µN V= 0 V	1 µm × 1 µm F_C = 6.28 µN V= 0 V	3 µm ×3 µm F_C = 0.39 µN V= 0 V	N_2 (RH < 0.5%)
			R = 1st scan	**E = 2nd-4th scan**	**R = 5th scan**	
Figure 5	p-Si	k = 3 N/m	1 µm × 1 µm F_C = 0.36 µN V = -1 V	1 µm × 1 µm F_C = 1.10 µN V = 0 V	2 µm × 2 µm F_C = 0.36 µN V = -1 V	Air (RH: ≈ 60 %)
			R = 1st scan	**E = 2nd scan**	**R = 3rd scan**	
Figure 6	p-Si	k = 27 N/m	- - -	0.5 µm × 0.5 µm F_C = 2.35 µN V = 0 V	1.5 µm × 1.5 µm F_C = 0.39 µN V = -0.5 V	N_2 (RH ≈ 0.5%)
			R = 1stscan	**E = 2nd scan**	**3rd scan**	
Figure 7	2 nm TiO_2/ nSi	k = 3 N/m	1 µm × 1 µm F_C = 0.51 µN V= 0 V	1 µm × 1 µm F_C = 1.10 µN V= 0 V	3 µm ×3 µm F_C = 0.51 µN V= 0 V	Air (RH ≈ 60 %)

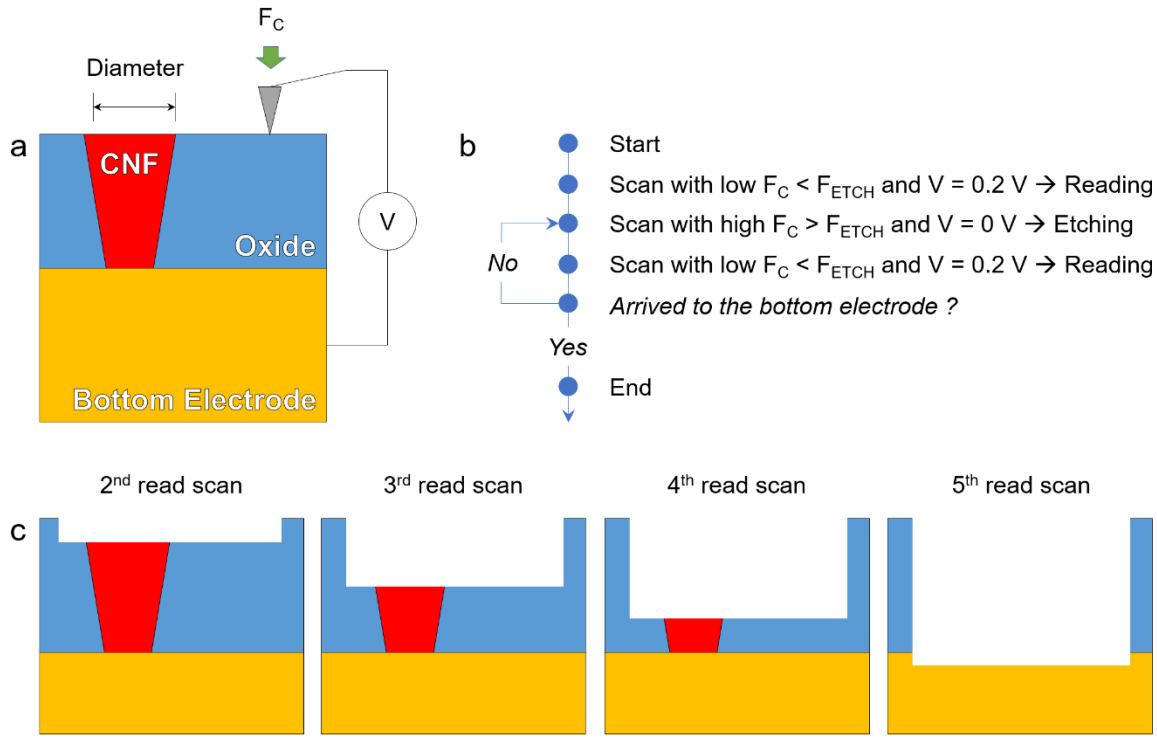

Figure 1. a) Schematic of scalpel AFM working principle when used to characterize the electrical properties of CNFs across an oxide in 3D. b) Recommended sequence of scans to be used in scalpel AFM experiments. It is important that the reading scans are collected applying low F_C, so that other sources of current (e.g., flexoelectricity, piezoelectricity) are avoided. It is also recommended that the lateral size of the reading scans is always a bit larger than the etching scans, so that the edge can be detected and the depth of each slice can be accurately confirmed. c) Schematics displaying the etching process step-by-step.

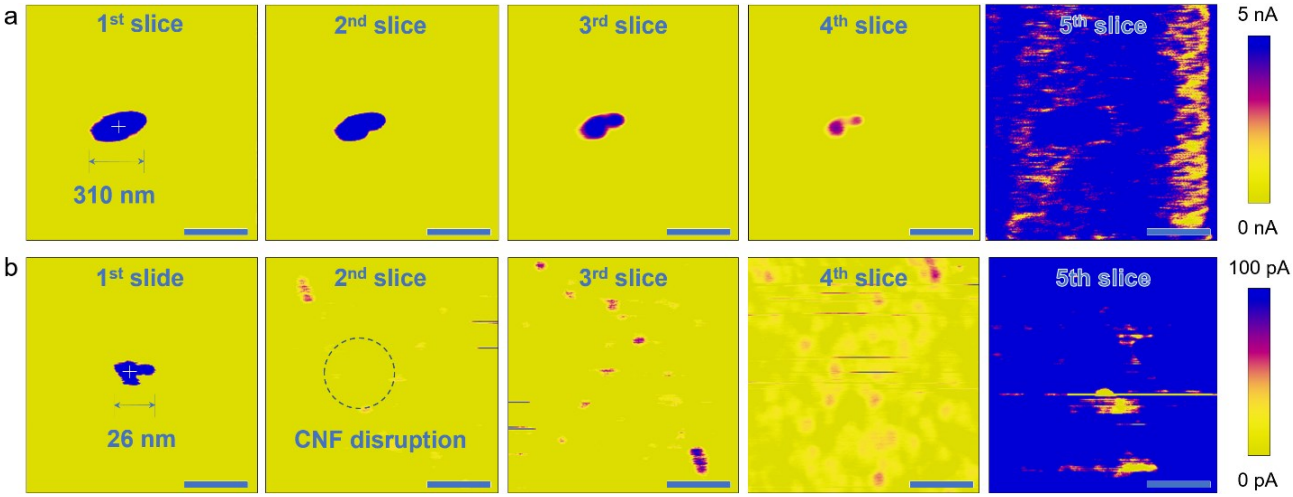

Figure 2. 3D characterization of CNFs formed with the tip of the CAFM by applying an I–V curve at two different locations of a 5 nm Al_2O_3/Au/Ti/SiO_X/n^{++}Si sample, using a) CL = 1 mA and b) CL = 10 µA. In both cases, five reading scans (slices) have been collected by applying F_C = 0.39 µN and V = −0.2 V. Between the slices, two etching scans applying F_C = 2.35 µN and V = 0 V have been applied. See more experimental details in Table 2. The vertical distance between the slices is ≈1.25 nm. The scale bars in (a) and (b) are 400 and 40 nm (respectively). The location where the I–V curves were applied have been highlighted with a white cross in the 1st slices. In both cases the I–V curves show linear conduction in the backward I–V curve (see Supporting Information Figure S2) indicating that the CNF has been completely formed.

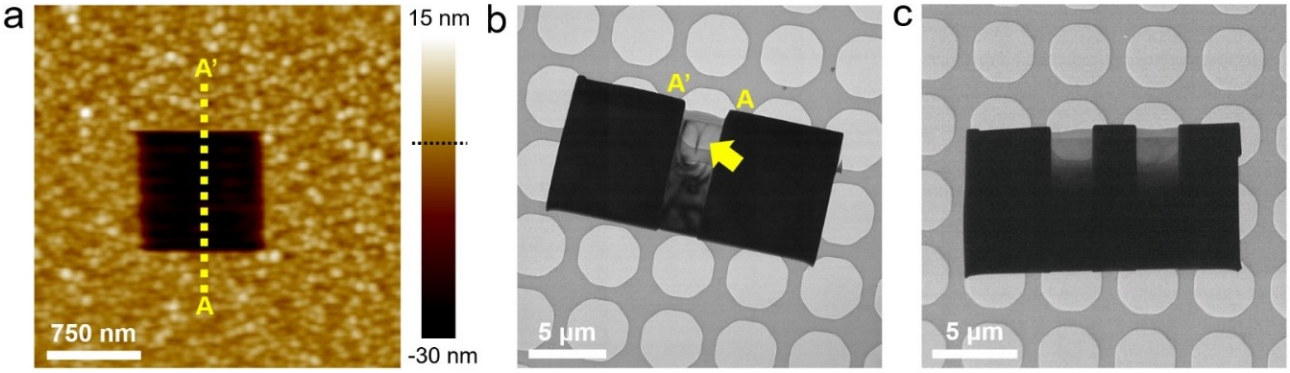

Figure 3. 3 µm × 3 µm (reading) topographic image collected on the surface of a 50 nm Al_2O_3/Au/Ti/SiO_X/n^{++}Si sample where a 1 µm × 1 µm etching scan was previously applied (see more experimental details in Table 2). The A–A′ yellow dashed line indicates the cut done with FIB. b) TEM image of the lamella cut at the region indicated with A–A′ in panel (a); the lamella is on a Cu grid typical for TEM inspection. c) similar lamella cut in a sample where no etching has been applied. The lamella in (b) has one thin area, while the lamella in (c) has two thin areas. Only the lamellas' cuts at the regions that have been etched with the CAFM show a dark trace propagating to the substrate, as indicated by the yellow arrow in panel (b).

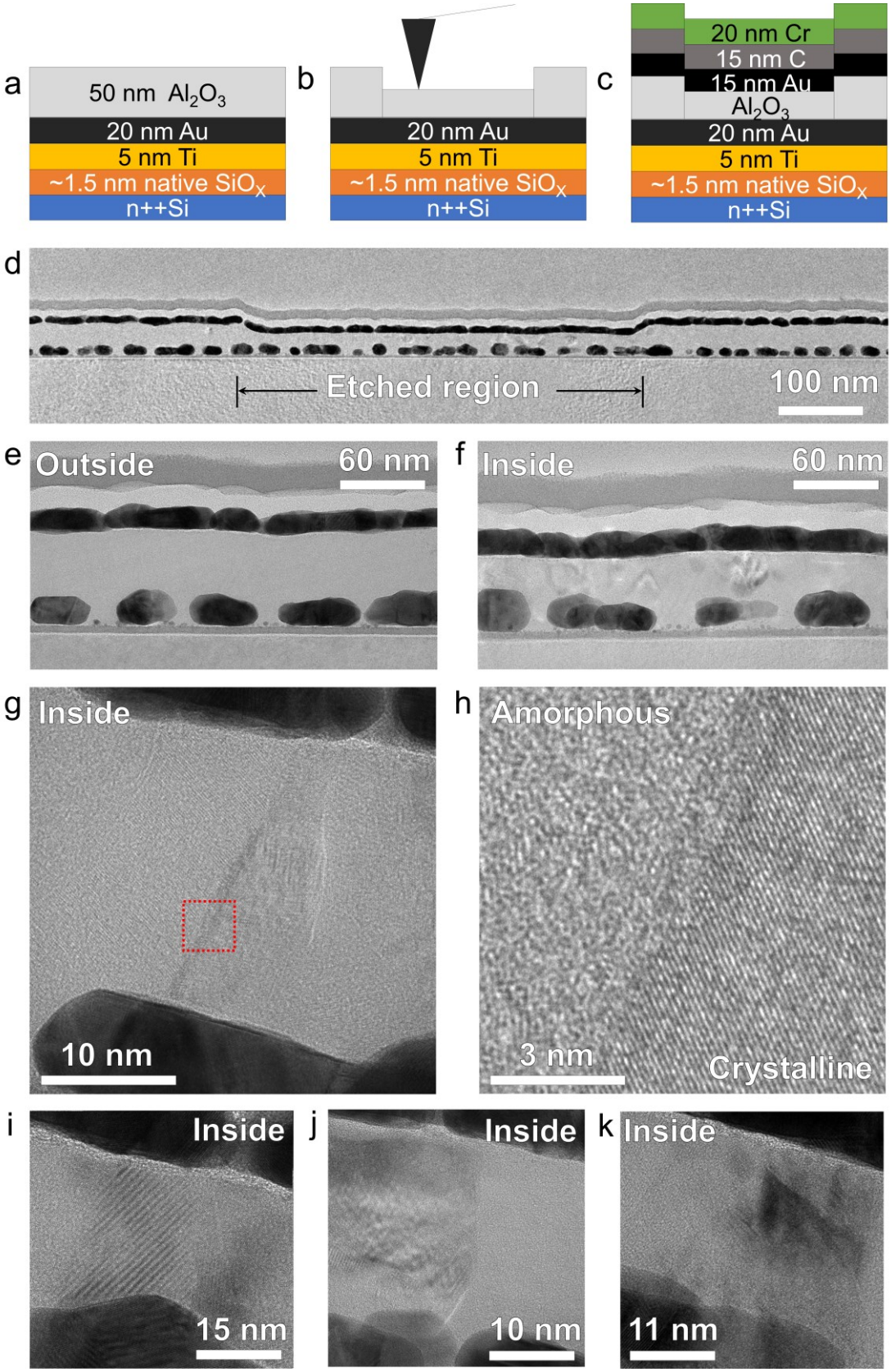

Figure 4. Panels (a)–(c) show the etching and sample preparation process before FIB and TEM experiments. d) Cross-sectional TEM image of the Cr/C/Au/Al_2O_3/Au/Ti/SiO_X/n^{++}Si sample across the A–A' section line shown in Figure 3a. e,f) Zoom in cross-sectional TEM images of different locations of the sample outside and inside the etched region. g–k) show different morphologies only

observed inside the etched area. Panels (g)–(i) show phase change, panel (j) shows severe defect formation, and panel (k) shows metal penetration. Panel (h) has been collected at the red squared area in panel (g). Overall, the images reveal that CAFM tomography severely modifies the atomic structure of the Al_2O_3 film at the etched region.

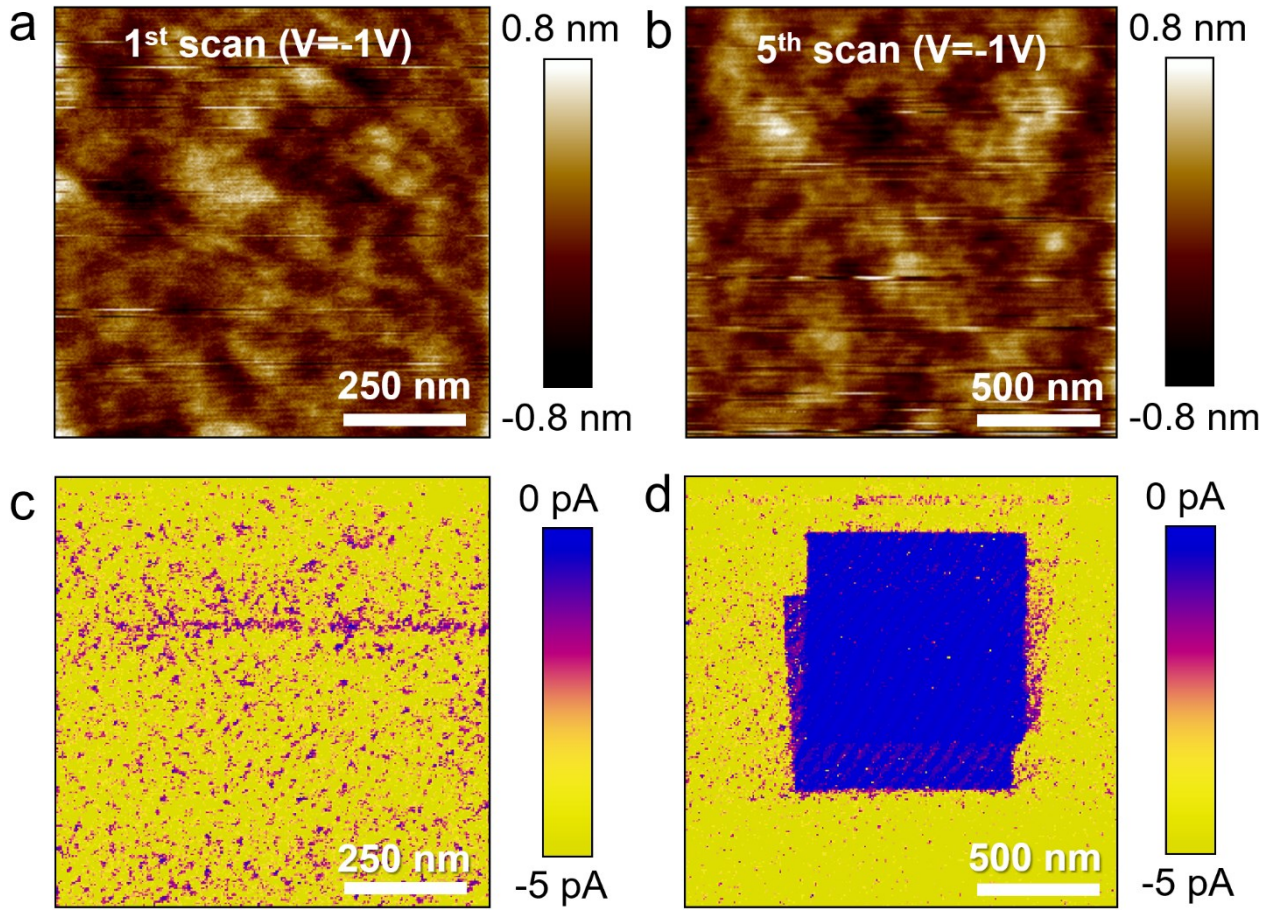

Figure 5. a,b) Topographic and c,d) current maps collected during the a,c) 1st and b,d) 5th scans, within a sequence of five scans, collected at the same location on a pSi sample. During the 1st and 5th scans F_C = 0.36 µN and V = −1 V (to characterize the sample), and during the 2nd–4th scans F_C = 1.10 µN (to try to etch the sample). This was measured in a Multimode V AFM working in air atmosphere using a long-cantilever solid B-doped diamond tip (see more experimental details in Table 2). The CAFM scans did not etch the surface of the sample (due to the low spring constant of the long-cantilever tip used), but the pressure applied was high enough to change the electrical properties of the pSi sample.

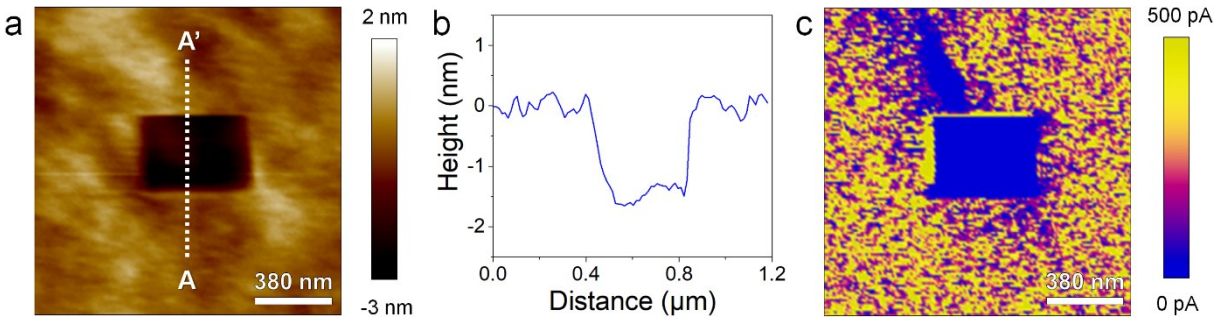

Figure 6: (a) 3μm × 3 μm topographic map of pSi (applying F_C = 0.39 μN and V = -0.5 V) after etching using B-doped solid diamond tip with a short-cantilever solid B-doped diamond tip (applying F_C = 2.35 μN and V = 0 V). See more experimental details in Table 2. The depth of the etched area is ~1.5 nm. (b) Cross section collected at the A-A' line highlighted in (a). (c) Current map collected simultaneously to (a). The etched region is much more insulating than the fresh one. The pSi sample has been immersed in HF for 10 s and washed with pure water right before the etching experiment to remove the native oxide.

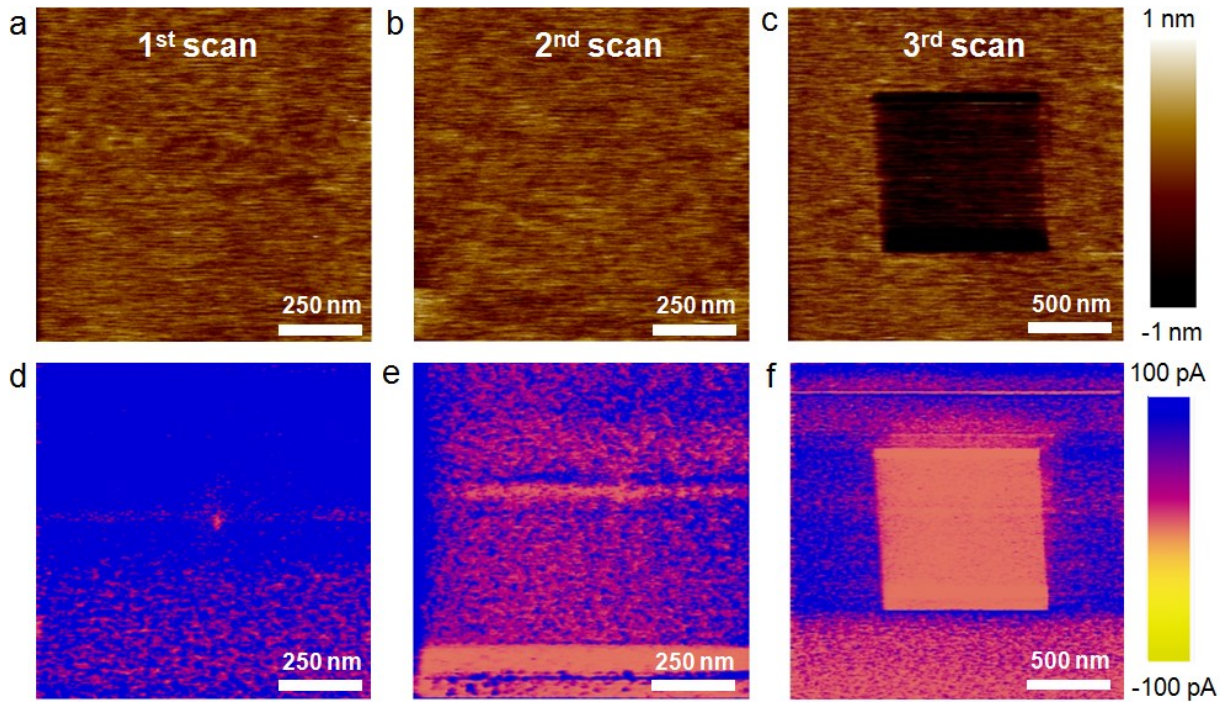

Figure 7. a–c) Topographic and d–f) current maps collected during the a,d) 1st, b,e) 2nd, and c,f) 3rd scans of a sequence of three scans on the sur-face of a 2 nm TiO_2/nSi sample, by applying F_C of 0.51, 1.10, and 0.51 μN (see more experimental details in Table 2). The etched area is ≈1 nm deep (see Figure S9, Supporting Information). Panel (f) indicates that the etching modified the electrical properties of the TiO_2 film.

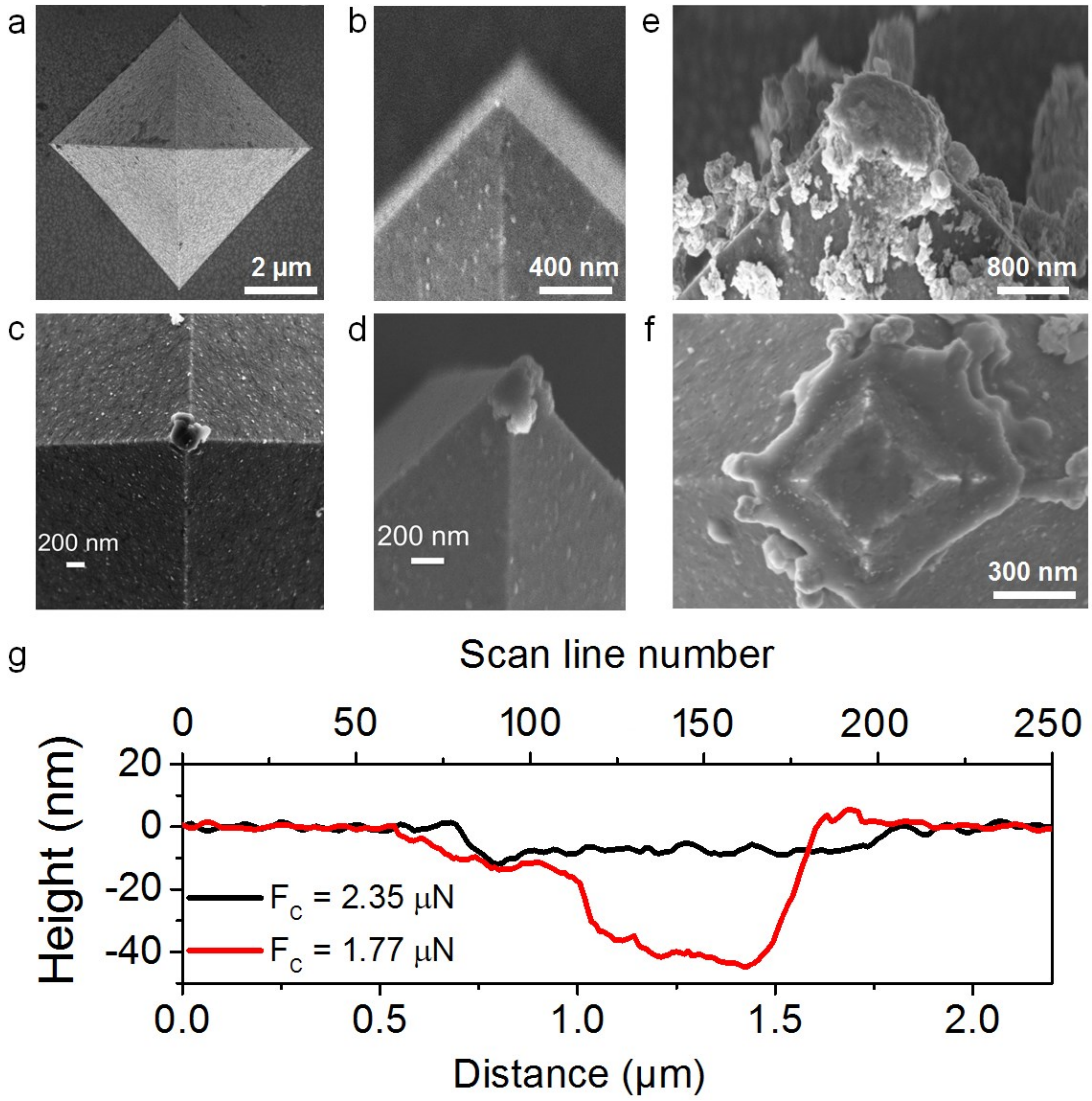

Figure 8. a) Top and b) side view SEM images of a pristine B-doped solid diamond probe. The apex is very sharp, with a radius of curvature of tens of nm. c) Top and d) side view SEM image of a B-doped solid diamond probe after etching the surface of sputter-deposited SiO_X by applying 12 scans with size 2 µm × 2 µm, F_C = 3.5 µN, and scanline density of 256 lines per scan plus 12 scans more with size 2 µm × 2 µm, F_C = 7.1 µN, and scanline density of 256 lines per scan. The total distance scanned is 18 mm. This probe shows an electrical resistance 7 kΩ higher and an etching rate 20% higher than the same tip when it was new. Panels (e) and (f) show top view SEM images of B-doped solid diamond probes that have been degraded by particles adhesion and apex blunting (respectively). The experiments in panels (a)–(f) have been carried out in a Dimension Icon AFM from Bruker under air atmosphere. g) Black line: cross-section of a zoom out (2.5 µm × 2.5 µm) topographic map measured with F_C = 0.39 µN on an Al_2O_3 region that was previously etched by applying two 1 µm × 1 µm scans using F_C = 2.35 µN. Red line: same experiment performed on another region of the Al_2O_3 sample, but using an F_C = 1.77 µN during the etching. The experiments have been done with the same CAFM tip, which was not new at the moment of starting the experiment, and the experiments performed to obtain the black line were performed before those to collect the red line. Both experiments were carried out in a Multimode V AFM from Veeco working in air atmosphere. Surprisingly, the experiment performed at lower FC shows sudden increase of the etching rate. The only feasible explanation is that one particle detached from the tip, leading to a smaller A_C and larger etching rate.

Supplementary Information

On the Limits of Scalpel AFM for the 3D Electrical Characterization of Nanomaterials

*Shaochuan Chen, Lanlan Jiang, Mark Buckwell, Xu Jing, Yanfeng Ji, Enric Grustan-Gutierrez, Fei Hui, Yuanyuan Shi, Mathias Rommel, Albena Paskaleva, Guenther Benstetter, Wing H. Ng, Adnan Mehonic, Anthony J. Kenyon and Mario Lanza**

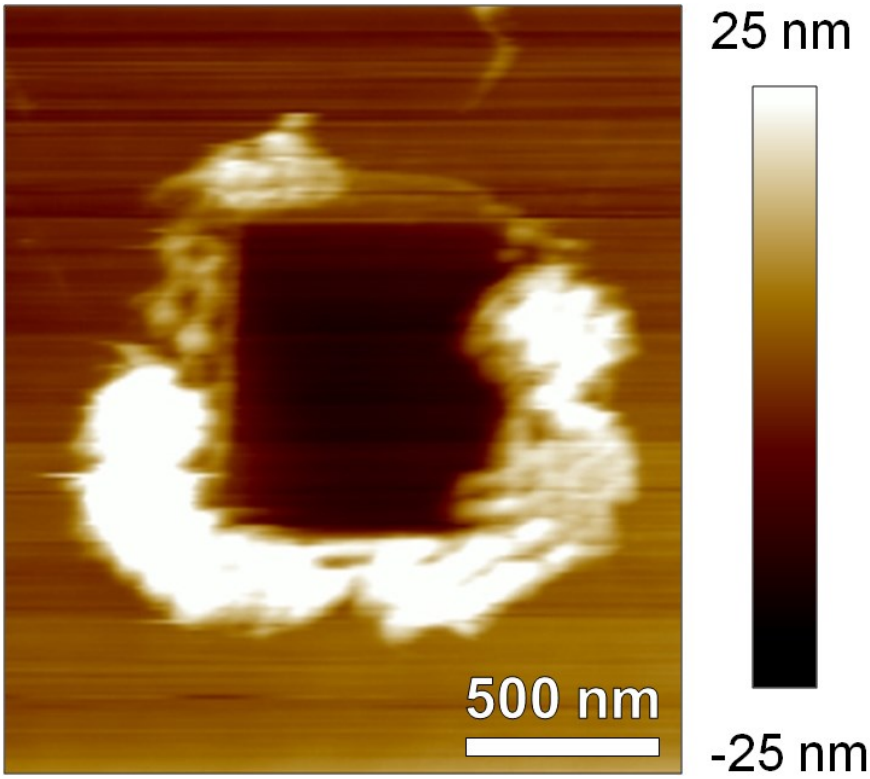

Figure S1: Zoom out topographic map collected on the surface of pSi, at a location of the sample that was previously etched using a B-doped solid diamond tip with k = 27 N/m. The accumulation of debris on the sides of the sample is very clear.

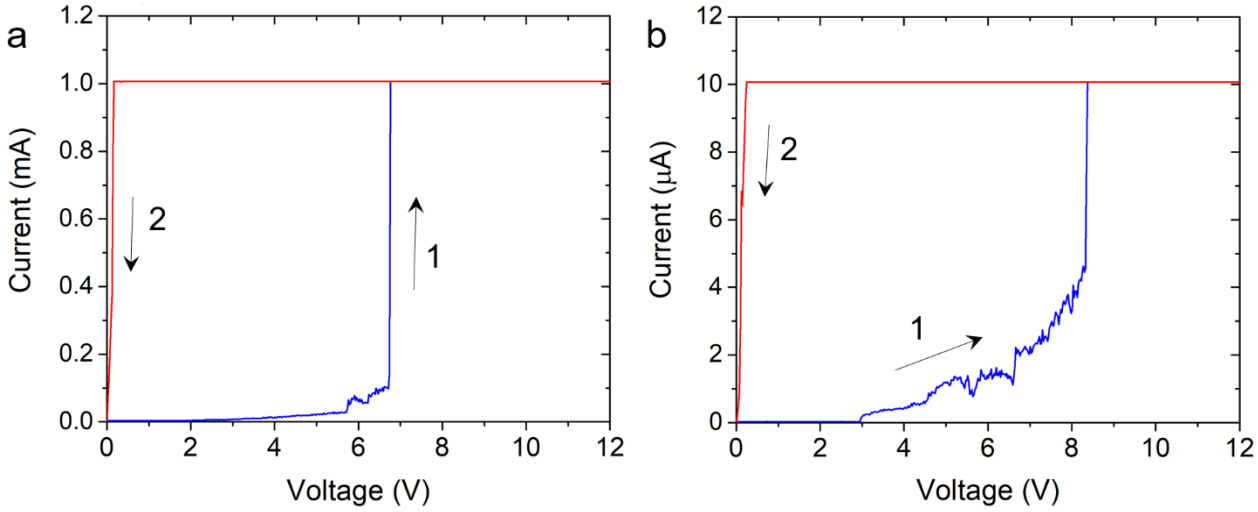

Figure S2: Forward and backward I-V curves collected with the tip of the CAFM on the suface of the 5 nm Al_2O_3/Au/Ti/SiO_X/n^{++}Si sample using (a) CL = 1 mA and (b) CL = 10 μA. These I-V curves have been collected prior to the scalpel AFM experiments shown in Figure 2 of the main text.

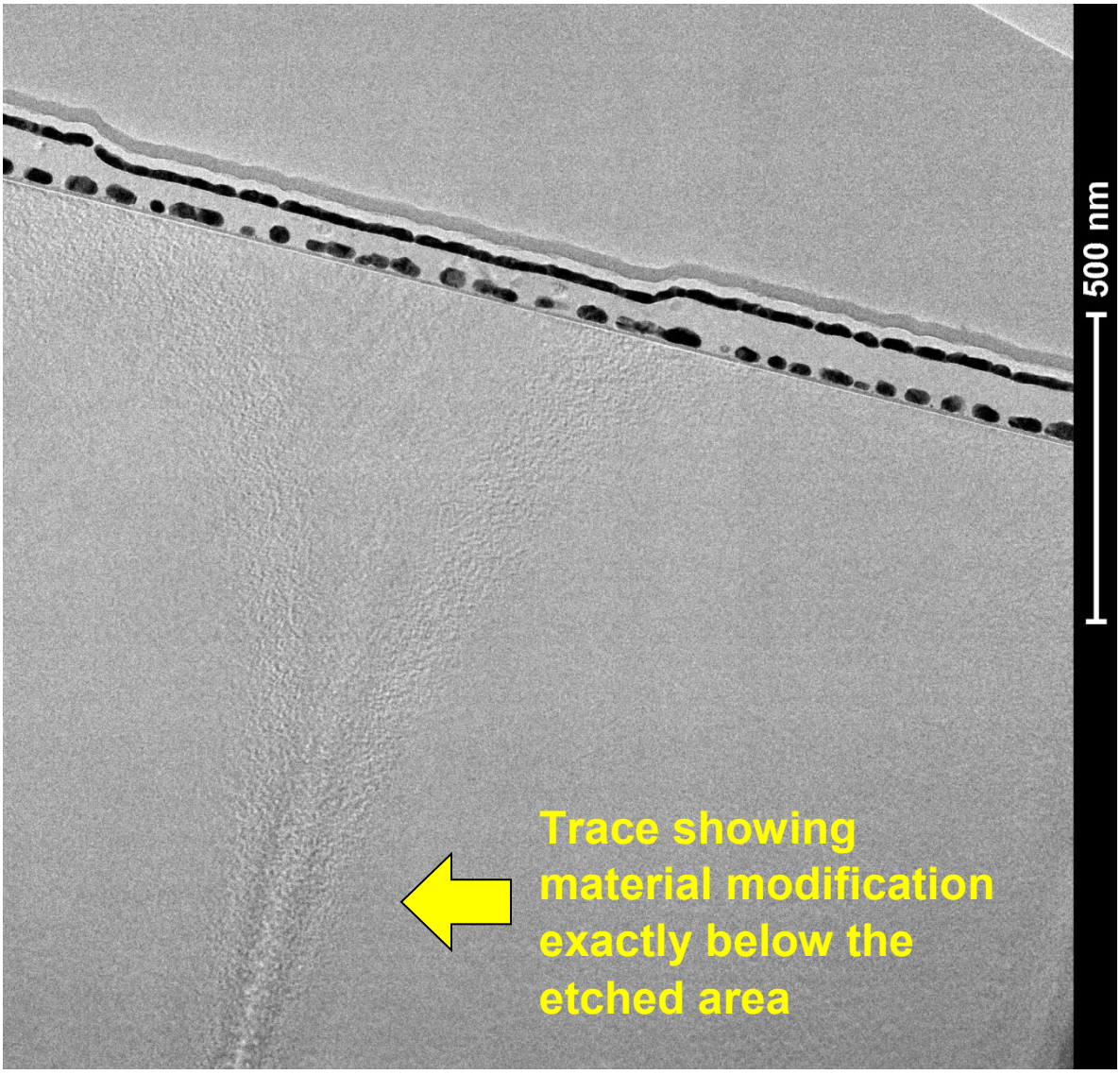

Figure S3: Original cross sectional TEM image for Figure 6d of the main text. The image clearly shows a trace right below the etched area.

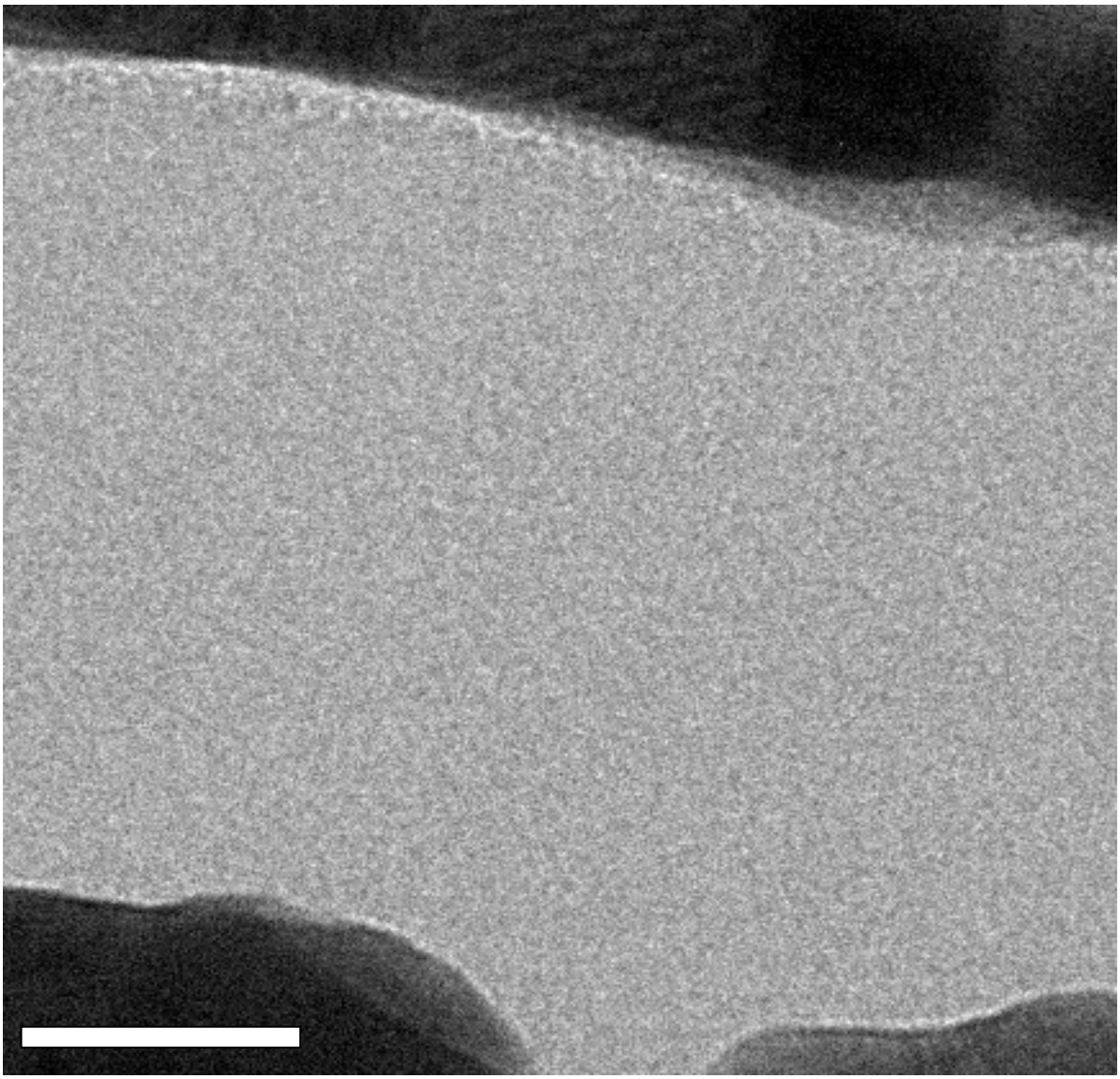

Figure S4: Zoom in image for Figure 6e in the main text showing the perfect amorphous structure of the fresh Al_2O_3 layer, i.e. outside the etched region. The scale bar is 15 nm.

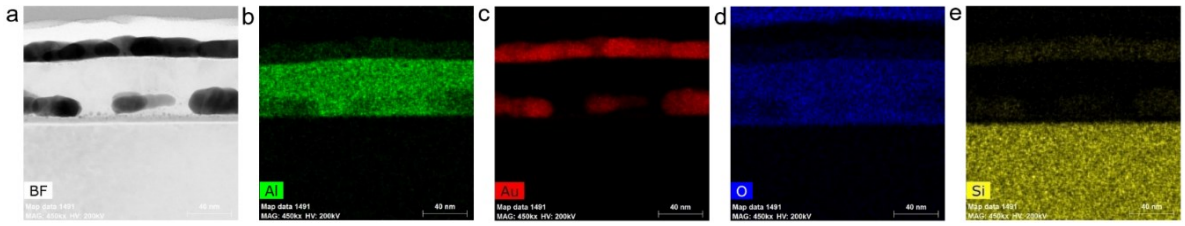

Figure S5: EDS analysis of Al, Au, O and Si elements in a 50 nm Al_2O_3/20 nm Au/5 nm Ti/n^{++}Si sample that has been exposed to CAFM tomography

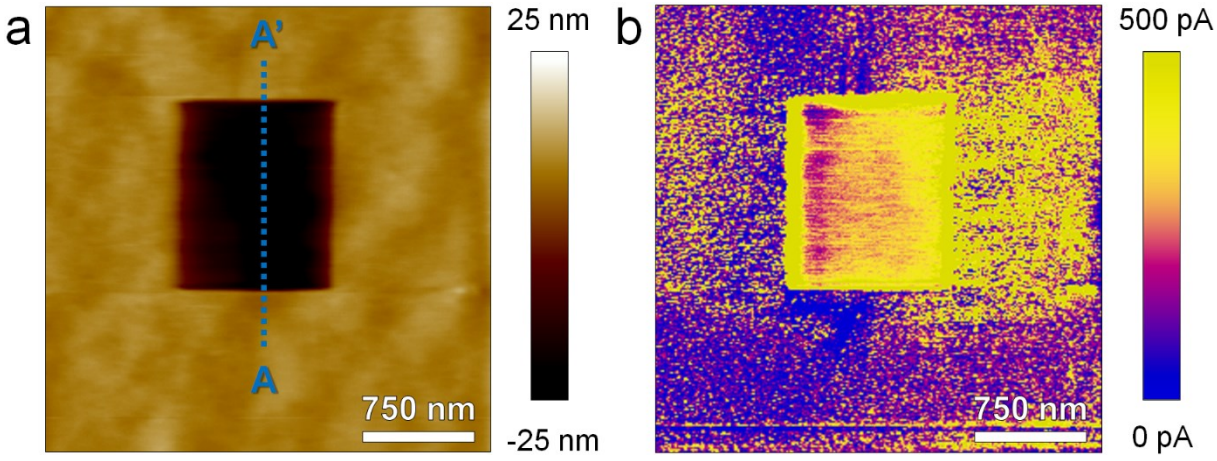

Figure S6: Etching of a pSi wafer with its native SiO_X. The current profile of the etched area is different than that observed in Figure 6c of the main text.

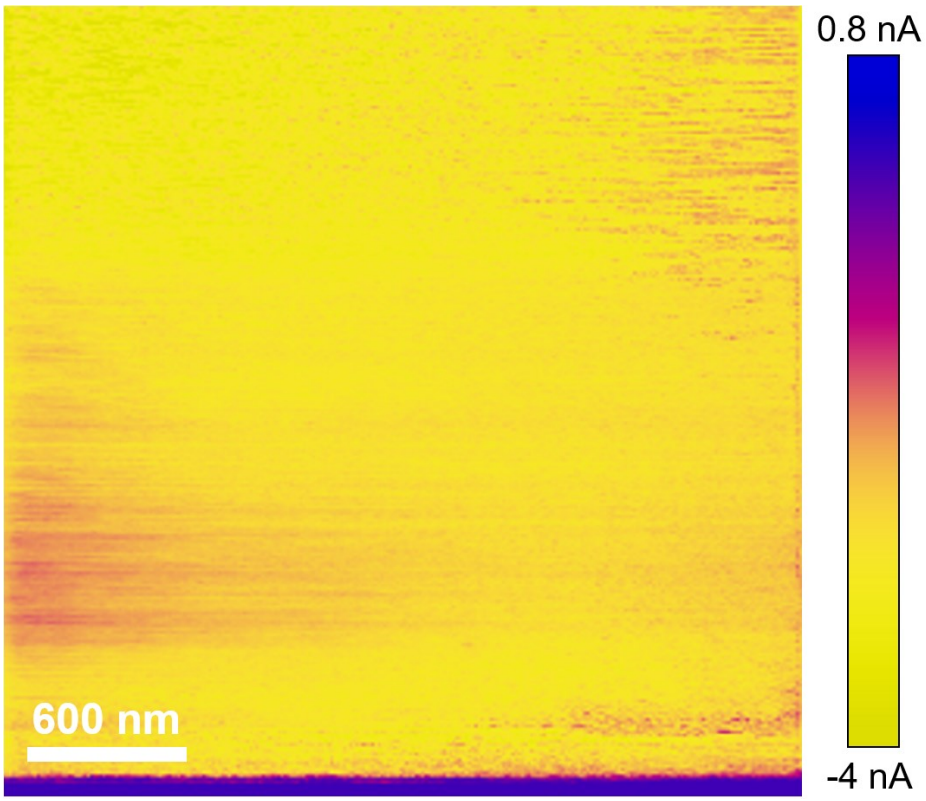

Figure S7: Current map obtained on pSi with high F_C = 6.28 µN and bias 0 V showing very high currents.

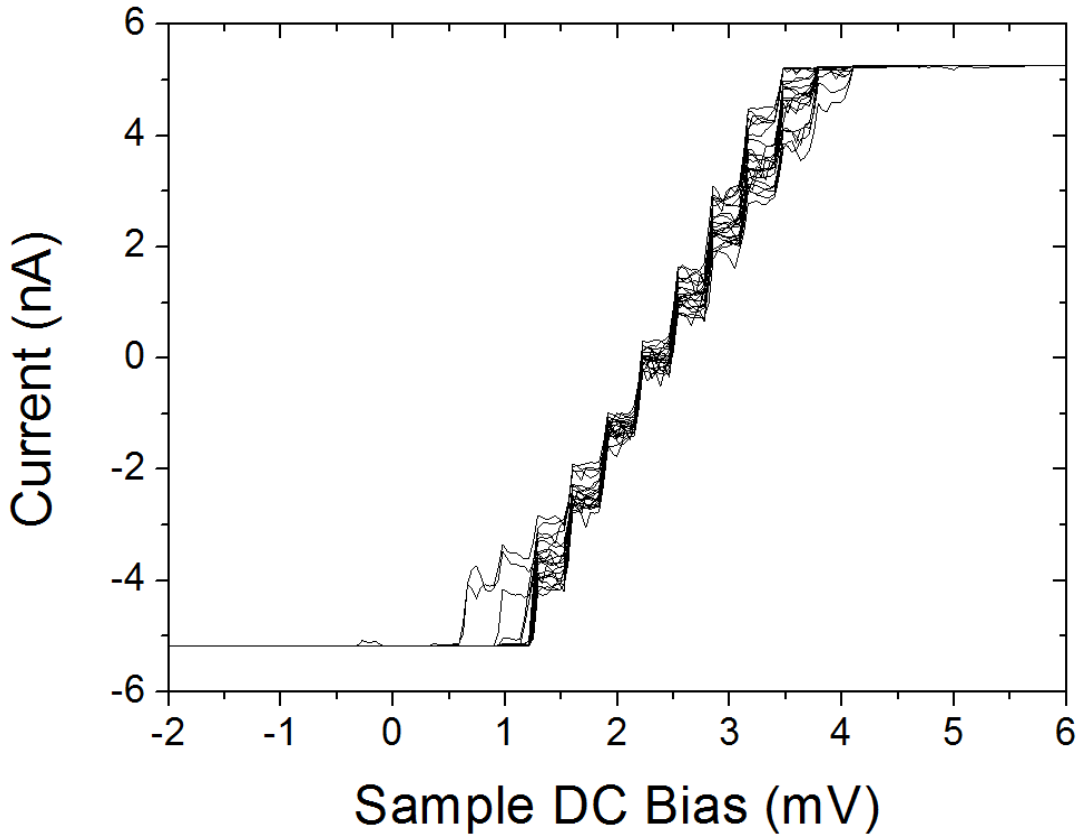

Figure S8: Ten I-V curves collected with the CAFM using a metallic substrate. As it can observed, the offset of our CAFM is 2.25 mV (that is the voltage at which the current is zero). This voltage is very low and unable to produce the large currents observed in Figure S7 when measuring pSi.

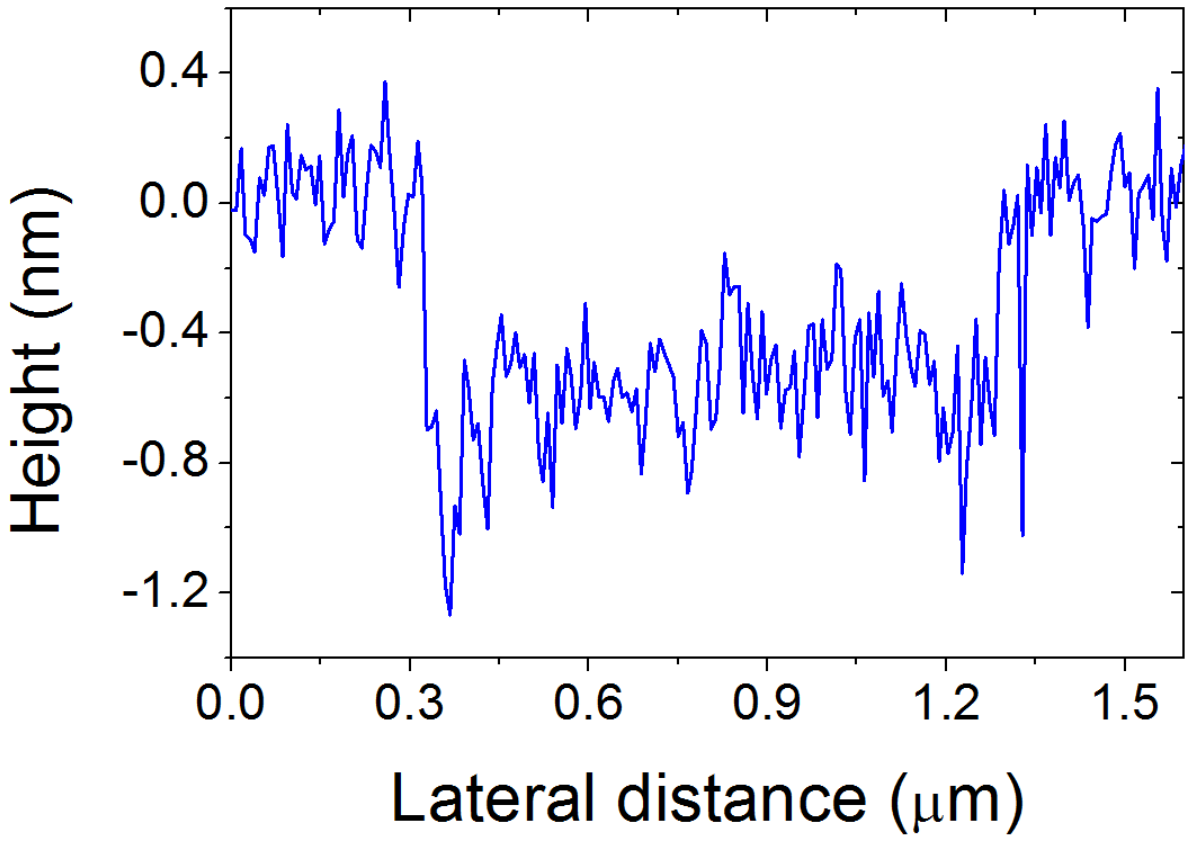

Figure S9: Cross section analysis of the topographic AFM map shown in Figure 7c. The cross section has been carried out at the center of the image (vertically).

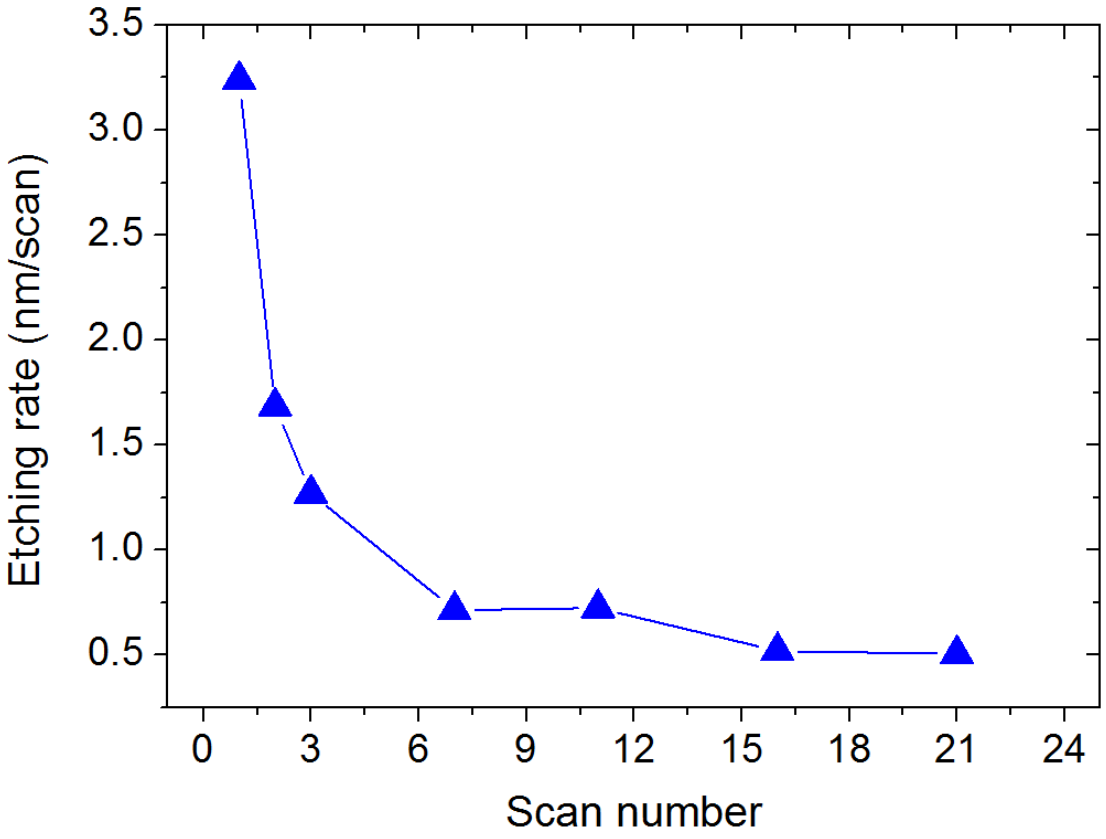

Figure S10: Etching rate depending on the number of scans for a diamond tip with $k = 80$ N/m (typical) when etching the surface of a SiO_X wafer with the same F_C. The etch rate decreases rapidly as the number of scans increases.